Longitudinal transcriptomics define the stages of myeloid activation in the living human brain after intracerebral hemorrhage

HHS Public Access

Author manuscript

Sci Immunol. Author manuscript; available in PMC 2021 August 19.

Published in final edited form as:

Sci Immunol. 2021 February 19; 6(56): . doi:10.1126/sciimmunol.abd6279.

Longitudinal transcriptomics define the stages of myeloid activation in the living human brain after intracerebral hemorrhage

Michael H. Askenase[#1,2], **Brittany A. Goods**[#3,4,5,6], **Hannah E. Beatty**[1,2], **Arthur F. Steinschneider**[1,2], **Sofia E. Velazquez**[1,2], **Artem Osherov**[1,2], **Margaret J. Landreneau**[1,2], **Shaina L. Carroll**[3,4,5,6], **Tho B. Tran**[1,2], **Victor S. Avram**[1,2], **Riley S. Drake**[3,4,5,6], **G. James Gatter**[3,4,5,6], **Jordan A. Massey**[1,2], **Saravanan S. Karuppagounder**[7,8], **Rajiv R. Ratan**[7,8], **Charles C. Matouk**[9], **Kevin N. Sheth**[9], **Wendy C. Ziai**[10,11], **Adrian R. Parry-Jones**[12,13], **Issam A. Awad**[14], **Mario Zuccarello**[15], **Richard E. Thompson**[10,16], **Jesse Dawson**[17], **Daniel F. Hanley**[10], **J. Christopher Love**[#4,5,18,*], **Alex K. Shalek**[#3,4,5,6,*], **Lauren H. Sansing**[#1,2,19,*], **MISTIE III Consortium**[#‡], **ICHseq investigators**[‡]

[1]Department of Neurology, Yale School of Medicine, New Haven, Connecticut, USA

[2]Department of Immunobiology, Yale School of Medicine, New Haven, Connecticut, USA

[3]Institute for Medical Engineering & Science (IMES) and Department of Chemistry, MIT, Cambridge, Massachusetts, USA

[4]Koch Institute for Integrative Cancer Research, MIT, Cambridge, Massachusetts, USA

[5]Broad Institute of MIT and Harvard, Cambridge, Massachusetts, USA

[6]Ragon Institute of MGH, MIT and Harvard, Cambridge, Massachusetts, USA

[7]Sperling Center for Hemorrhagic Stroke Recovery, Burke Neurological Institute at Weill Cornell Medicine, White Plains, New York, USA

[8]Feil Family Brain and Mind Research Institute, Weill Cornell Medicine, New York, New York, USA

[9]Department of Neurosurgery, Yale School of Medicine, New Haven, Connecticut, USA

[10]Division of Brain Injury Outcomes, Johns Hopkins University, Baltimore, Maryland, USA

[11]Departments of Neurology, Neurosurgery, and Anesthesiology/Critical Care Medicine, Johns Hopkins, Baltimore, Maryland, USA

[*]Corresponding authors: lauren.sansing@yale.edu, shalek@mit.edu, clove@mit.edu.

[‡]Author lists for MISTIE III Consortium and ICHseq investigators can be found in the Supplementary Materials.

Author contributions

LHS designed the study in consultation with DFH, JCL, MHA, and BAG. LHS, AKS, and JCL supervised the study at all stages. Sample processing and cell sorting were performed by MHA, HEB, AFS, MJL, and TBT. BAG isolated RNA, generated cDNA libraries, and executed transcriptional sequencing with assistance from SLC and RSD. MHA designed and performed the transcriptional analysis with assistance from VSA, BAG, JG, and AKS. *In vitro* assays were designed by MHA, LHS, SSK, and RRR, and performed by HEB, AO, SEV, MHA, TBT, and JAM. CCM and KNS contributed to *in vitro* studies of effects of rtPA on gene expression. DFH, IAA, MZ, WZ, ARP, RET, and JD led key aspects of the MISTIE III trial and provided trial data for this study. MHA, BAG, JCL, AKS, and LHS wrote the manuscript with critical input from all authors.

Competing Interests

DFH reports compensation for consulting from BrainScope, Neurotrope, Op2Lysis, and Portola Pharmaceuticals.

[12]Division of Cardiovascular Sciences, School of Medicine, Faculty of Biology, Medicine, and Health, University of Manchester, Manchester Academic Health Science Centre, Manchester, UK

[13]Manchester Centre for Clinical Neurosciences, Salford Royal National Health Service Foundation Trust, Manchester Academic Health Science Centre, Salford.

[14]Neurovascular Surgery Program, Section of Neurosurgery, The University of Chicago Pritzker School of Medicine, Chicago, Illinois, USA

[15]Department of Neurosurgery, University of Cincinnati College of Medicine, Cincinnati, Ohio, USA

[16]Department of Biostatistics, School of Public Health, Johns Hopkins University, Baltimore, Maryland, USA

[17]Institute of Cardiovascular and Medical Sciences, University of Glasgow, Glasgow, UK

[18]Department of Chemical Engineering, Koch Institute for Integrative Cancer Research, MIT, Cambridge, Massachusetts, USA

[19]Human and Translational Immunology Program, Yale School of Medicine

[#] These authors contributed equally to this work.

Abstract

Opportunities to interrogate the immune responses in the injured tissue of living patients suffering from acute sterile injuries such as stroke and heart attack are limited. We leveraged a clinical trial of minimally-invasive neurosurgery for patients with intracerebral hemorrhage (ICH), a severely disabling subtype of stroke, to investigate the dynamics of inflammation at the site of brain injury over time. Longitudinal transcriptional profiling of CD14+ monocytes/macrophages and neutrophils from ICH patient hematomas revealed that the myeloid response to ICH within the hematoma is distinct from that in the blood and occurs in stages conserved across the patient cohort. Initially, hematoma myeloid cells expressed a robust anabolic pro-inflammatory profile characterized by activation of hypoxia inducible factors (HIFs) and expression of genes encoding immune factors and glycolysis. Subsequently, inflammatory gene expression decreased over time, while anti-inflammatory circuits were maintained and phagocytic and anti-oxidative pathways upregulated. During this transition to immune resolution, glycolysis gene expression and levels of the potent pro-resolution lipid mediator prostaglandin E_2 remained elevated in the hematoma, and surprisingly these elevations correlated with positive patient outcomes. *Ex vivo* activation of human macrophages by ICH-associated stimuli highlighted an important role for HIFs in production of both inflammatory and anti-inflammatory factors, including PGE_2, which in turn augmented VEGF production. Our findings define the time course of myeloid activation in the human brain after ICH, revealing a conserved progression of immune responses from pro-inflammatory to pro-resolution states in humans following brain injury and identifying transcriptional programs associated with neurological recovery.

One Sentence Summary

RNA sequencing of cerebral hematoma myeloid cells reveals a two stage functional and metabolic program associated with recovery.

Introduction

The response to acute brain injuries—including intracerebral hemorrhage (ICH), ischemic stroke, and traumatic brain injury—involves a complex and coordinated network of cell types and secreted factors. The immune system plays a key role in mediating this response, with peripheral CD14+ monocytes and neutrophils rapidly recruited to the site of injury by chemotactic factors secreted by brain-resident microglia, astrocytes, and endothelial cells (1). Monocyte-derived macrophages and neutrophils can exacerbate initial damage to the brain as well as enhance neurological deficits (2). However, animal models of acute brain injury have demonstrated that neutrophils and macrophages can also ameliorate pro-inflammatory responses, initiate resolution of neuroinflammation, and promote neurological recovery (3–6). Thus, modulation rather than inhibition of myeloid immune responses may be a promising avenue for treatment of brain injuries. Due to the difficulty of accessing inflamed brain tissue in living patients, the contribution of recruited myeloid cells to both initial tissue damage and subsequent neurological recovery in patients is not well-defined, hampering efforts to therapeutically target these processes.

Recent studies in murine models have revealed the complexity and diversity of myeloid activation programs in central nervous system (CNS) inflammation (1, 7). The previous stratification of macrophages into “M1” inflammatory and “M2” anti-inflammatory phenotypes has been amended to a multi-dimensional model of macrophage polarization that incorporates a diverse range of inflammatory, anti-inflammatory, and reparative states (8–10). Important contributions of neutrophils to wound healing have become increasingly apparent (11). Additionally, transcriptomics and *in vitro* pharmacological inhibition of glycolytic and respiratory metabolic pathways have revealed the central role that glucose metabolism plays in shaping myeloid cell function (12–16). While these studies have highlighted the importance of myeloid metabolic states on function, they have predominantly been performed using the limited M1/M2 paradigm *in vitro* or in the context of immune responses to infection or cancer. How myeloid cell metabolism influences function during a complex sterile inflammatory response such as acute brain injury remains poorly understood (16, 17).

Acute sterile injuries such as heart attack and stroke are leading causes of death worldwide, but studying the role the immune system plays in the progression and outcomes of these diseases in patients is extremely challenging because the diseased tissue is typically only available post-mortem. To address this shortcoming, we launched ICHseq, a sub-study of the Minimally Invasive Surgery Plus Alteplase for Intracerebral Hemorrhage Evacuation (MISTIE III) surgical trial (18). The surgical approach tested in the trial, in which an indwelling catheter drained the cerebral hematoma over several days rather than the traditional single surgical evacuation of the hemorrhage, allowed for the daily collection of the hematoma effluent and matched peripheral blood samples. This provided an unprecedented opportunity to define the evolution of the myeloid immune response to brain hemorrhage over time in living patients.

Using longitudinal transcriptional profiling of CD14+ monocytes/macrophages and neutrophils isolated from the hematoma and peripheral blood samples, we show that the myeloid response within the hematoma is composed of two discrete stages. During the acute stage of the response (<4 days post-ICH), myeloid cells increased expression of glycolytic enzymes as well as a diverse array of pro- and anti-inflammatory factors. As the response entered the sub-acute stage (4 to 7 days post-ICH), inflammatory cytokine transcripts decreased in abundance in both cell types and CD14+ monocytes/macrophages acquire reparative and anti-oxidative. Higher expression levels of glycolytic enzymes and prostaglandin E synthase (*PTGES*) by CD14+ monocytes/macrophages during the sub-acute stage correlated with good patient outcomes at one year post-hemorrhage. E*x vivo* experiments using human macrophages confirmed that glycolysis supports production of PGE_2 by macrophages, which in turn augments secretion of VEGF. Overall, this work defines the myeloid transcriptional response within hematomas inside the brain parenchyma of living patients and suggests that glycolytic metabolism in macrophages may support neurological recovery after ICH.

Results

The myeloid response to ICH occurs in two stages.

We performed longitudinal transcriptional profiling of CD14+ monocytes/macrophages and neutrophils isolated from the hematoma effluent and peripheral blood of 21 patients enrolled in ICH-seq, a sub-study of the Minimally Invasive Surgery Plus Alteplase for Intracerebral Hemorrhage Evacuation (MISTIE III) trial (18) (Fig. 1A). As part of MISTIE III, a catheter was placed into the hematoma of ICH patients (occurring between 23 and 90 hours post-ICH onset in our cohort), followed by irrigation every 8 hours with recombinant tissue plasminogen activator (rtPA) to break down the clot and facilitate hematoma drainage. Hematoma effluent and matched peripheral blood were collected from ICH patients during catheter placement surgery, followed by daily collections of effluent and peripheral blood for up to an additional 4 days while the catheter was in place. Flow cytometry analysis of hematoma effluent revealed putative CD14+ monocyte/macrophage and CD66a/c/e+ granulocyte populations similar in proportion and surface protein signature to CD14+ “classical” monocytes and CD66a/c/e+ neutrophils in peripheral blood (Fig. S1, Fig. S2). We sorted these populations from each blood and hematoma sample by FACS (Fig. S2) and generated cDNA libraries for RNA sequencing, resulting in 139 monocyte/macrophage (82 blood, 57 hematoma) and 125 neutrophil (76 blood, 49 hematoma) profiles from the 21 enrolled patients, spanning 23 to 171 hours post-hemorrhage (Table S1). Our cohort included 13 males and 8 females (ages 29 to 77 years) with hematoma volumes of 26.37 to 85.65 mL (median = 63.0 mL) and Glasgow Coma Scale scores of 5 to 14 (median = 10) at the time of enrollment in MISTIE III. Additional characteristics of our patient cohort are provided in Tables S1 and S2.

To confirm the cellular identity of the sorted hematoma leukocyte populations, we first examined expression of specific lineage-specific transcripts. CD66a/c/e+ cells closely resembled neutrophils from the blood, expressing *CSF3R*, *CXCR1*, and *CXCR2* (Fig. S3A) while lacking expression of HLA molecules, eosinophil-specific *SIGLEC8*, and basophil-

specific *FCER1A* or *MS4A3*. Key lineage markers in CD14+ cells in the hematoma closely resembled that of circulating CD14+ monocytes. They expressed *CSF1R* and HLA molecules at high levels, and single sample gene set enrichment analysis (ssGSEA) revealed that their transcriptional profile more closely resembled CD14+ blood monocytes (19) than brain-resident microglia (20–22) (*P2RY12, TMEM119, GPR34*) or border-associated macrophages (23, 24) (*CD36*, *MRC1*, *AIF1*; Fig. S3B–E, Table S3). This led us to conclude that these cells were likely predominantly monocyte-derived; we henceforth refer to them as CD14+ monocytes/macrophages.

Principal component analysis on filtered and batch-corrected transcriptional data revealed that while myeloid populations in the peripheral blood of ICH patients clustered near those derived from healthy donor controls, cells isolated from hematoma separated from their blood counterparts along the first principle component (Fig. 1B). Differential gene expression results between healthy donor and ICH blood monocytes are provided in Table S4. Surprisingly, transcriptional profiles from either tissue did not show clear separation by patient (Fig. S4), indicating that patient-to-patient variability did not drive major variations in the overall myeloid transcriptional response.

To identify dynamic changes in the transcriptional programs of CD14+ monocytes/macrophages and neutrophils in hematoma over time after ICH, we first generated a cubic spline regression model of gene expression (25), incorporating time after ICH onset for each gene within each cell type. We then used k-means clustering to sort genes with significant changes over time into modules with shared temporal patterns of expression (Fig S5). This analysis revealed two distinct stages of gene expression in hematoma myeloid cells: an acute stage spanning approximately the first 4 days post-ICH, during which myeloid transcriptional profiles were rapidly changing, followed by a sub-acute stage spanning the remaining time interval of the study (4 to 7 days post-ICH) during which they were more stable (Fig. 1C).

We identified two prevailing patterns among dynamic genes in each cell type: one increasing in the acute stage before stabilizing after four days post-ICH (748 genes colored red in CD14+ monocytes/macrophages, 808 genes colored orange in neutrophils, adjusted $p < 0.05$) and the other decreasing in the acute stage before stabilizing (511 genes colored blue in CD14+ monocytes/macrophages, 665 genes colored teal in neutrophils, adjusted $p < 0.05$). While the two response stages were contemporaneous in monocytes and neutrophils, their transcriptional programs were distinct; just 205 differentially expressed genes (102 increasing expression over time, 103 decreasing expression) showed similar changes in expression in both cell types (Fig. 1D). Gene expression in the peripheral blood was comparatively stable, with just 7 genes in monocytes and 43 genes in neutrophils demonstrating significant changes in expression over time (Table S5). This two-stage dynamic myeloid response was highly conserved across our patient cohort (Fig S5D, H).

Myeloid cells activate a complex transcriptional state in the hematoma.

We next sought to define the myeloid transcriptional response during the acute stage of ICH by comparing the transcriptional profiles of hematoma CD14+ monocytes/macrophages and neutrophils to their peripheral counterparts in blood during the first four days post-ICH. To

do so, we analyzed the first hematoma and blood samples collected from each patient, which spanned between 23 and 99 hours post-ICH, using differential expression analysis by linear modeling (Materials and Methods) (25, 26). Both cell types demonstrated extensive transcriptional differences between the hematoma and blood: CD14+ monocytes/macrophages significantly increased expression of 1,865 genes and decreased expression of 3,008 genes when compared to blood monocytes ($p < 0.05$), while hematoma neutrophils increased expression of 1,504 genes and decreased expression of an additional 1,549 (Fig. 2A, Table S6). ssGSEA of Hallmark gene sets, a collection of genes curated to provide a comprehensive summary of key cellular pathways and functions (27), revealed a diverse array of immune signaling pathways activated in hematoma CD14+ monocytes/macrophages and neutrophils, including TGF-β, TNF-α, IL-2/STAT5, IL-6/JAK/STAT3, and PI3K/AKT/mTOR signaling (Fig. 2B). We also found enrichment in pathways related to cellular stress responses, including hypoxia and the unfolded protein response suggesting activation of hypoxia inducible factors (HIFs) and ATF4, known downstream effectors of increased mTOR activation. While neutrophil activation was dominated by immune-specific pathways, CD14+ monocytes/macrophages demonstrated a broader remodeling of cellular processes, including hemorrhage-related pathways such as complement activation, angiogenesis, and coagulation.

Recent studies have revealed complex transcriptional states for CD14+ monocytes/macrophages *in vivo* that do not correspond with “M1” or “M2” activation states previously defined predominantly by *in vitro* studies (8–10). Therefore, to perform a more nuanced evaluation of macrophage activation after ICH, we compared the transcriptional signatures of CD14+ monocytes/macrophages in blood and hematoma using gene set enrichment analysis (GSEA) for 49 transcriptional modules identified in activated macrophages in response to a wide array of *in vitro* stimuli (13) (Table S7). The transcriptional profiles of hematoma CD14+ monocytes/macrophages did not show enrichment for gene modules typically induced by either M1 or M2 conditions, but were significantly enriched for three others: modules 16 and 21 associated with fatty acid stimulation, and module 30 associated with combined stimulation of TNF, PGE_2, and TLR2. Hematoma CD14+ monocytes/macrophages also upregulated pathways controlling cholesterol lipid homeostasis (Fig. 2B), an essential feature of the microglia transcriptional program (20, 28). Augmented expression of cholesterol processing pathways has also been reported in myeloid cells found in the CSF of HIV patients (29) and macrophages found in the perivascular space, meninges, and choroid plexus of mouse brains (23), suggesting that the enrichment of lipid-stimulated transcriptional modules may represent adaptation to the cholesterol-rich CNS environment that occurs regardless of the inflammatory setting. By contrast, increased activity of cytokine signaling pathways in both CD14+ monocytes/macrophages and neutrophils likely occurs in response to local inflammation caused by ICH. Thus, CD14+ monocytes/macrophages and neutrophils acquire distinct transcriptional states during the acute stage of ICH in response to immune and tissue-derived signals within the hemorrhaged brain. Differential expression and longitudinal expression analyses can be further explored interactively using the ICH-seq online tool (https://ichseq.sansinglab.research.yale.edu/).

Myeloid cell transcriptomics reveal metabolical and functional reprogramming during the acute stage of ICH.

CD14+ monocytes/macrophages and neutrophils in the hematoma displayed transcriptional signatures indicative of extensive transcriptional remodeling of glucose metabolism in conjunction with activation (Fig. 2B, Fig. 3). Canonical pathway analysis of differentially expressed genes between blood and hematoma cells during the acute stage revealed glycolysis as the single most upregulated pathway in both cell types within the hematoma ($p<0.001$) (Fig. 3A). Additionally, predictive "Genes and Metabolites" (GAM) metabolic modeling (30) uncovered a central role for glycolysis in metabolic reprogramming in CD14+ monocytes/macrophages (Fig. S6). GAM modeling further revealed changes to pathways controlling synthesis of eicosanoids, lipid mediators that direct macrophage responses during tissue injury. Combined, these data suggest extensive transcriptional reprogramming of myeloid cell metabolism in the hematoma milieu that may modulate their functions during this period.

To better characterize glucose metabolism and myeloid function during the acute stage of ICH, we first examined the expression of glucose transporters GLUT1 and GLUT3 (encoded by *SLC2A1* and *SLC2A3* respectively) as well as enzymes involved in the three major pathways of glucose utilization: glycolysis, the citric acid (TCA or Kreb's) cycle, and the pentose phosphate pathway (PPP). CD14+ monocytes/macrophages and neutrophils both significantly upregulated glucose transporters and nearly every enzyme in the glycolysis pathway (Fig. 3B). By contrast, both cell types decreased expression of TCA cycle genes (Fig. 3C) and, surprisingly, the enzymes controlling the PPP (Fig. 3D), which have previously been reported to mirror expression of glycolytic enzymes in myeloid activation (31–33). These metabolic changes were conserved across patients (Fig S7).

Transcriptional reprogramming of glucose metabolism in the hematoma during the acute stage of ICH was concurrent with increased expression of secreted protein and lipid immune factors. Both CD14+ monocytes/macrophages and neutrophils increased expression of inflammatory cytokine genes such as *IL6*, *IL1A*, and *IL1B* as well as anti-inflammatory and neuroprotective factors such as *IL10* and *LIF* (Fig. 3E, Fig. S6); chemokine genes were also upregulated, mostly by CD14+ monocytes/macrophages (Fig. 3F). A closer examination of eicosanoid synthesis (Fig. 3G) revealed increased expression of genes encoding enzymes responsible for generation of anti-inflammatory PGE_2 (*MGLL*, *PTGS2*, *PTGES*) concurrent with downregulation of genes encoding enzymes responsible for production of inflammatory thromboxanes and leukotrienes (*TBXAS1*, *LTA4H*, *ALOX5*, *ALOX15B*). Upstream regulator analysis of differentially expressed genes predicted activation of a suite of factors known to modulate glucose metabolism, including N-Myc and, in particular, HIFs: HIF1-α, HIF2-α, and their shared co-factor ARNT (HIF-1β). NUPR1, a transcription factor that regulates metabolic adaptation to ER stress and is closely tied to HIF activation (34, 35), was also predicted to be activated (Fig. 3H). HIF signaling controls a metabolic switch to anabolic metabolism in neutrophils and macrophages in a broad range of inflammatory settings by augmenting glycolytic generation of molecular building blocks that support lipid synthesis and inflammatory cytokine secretion (14, 36–38).

Expression of glycolytic and inflammatory genes diminish over time in hematoma myeloid cells.

We next investigated how the transcriptional profiles of myeloid cells in the hematoma changed over time. Gene ontology analysis of genes decreasing in expression over time as identified by spline regression (Figure 1C) suggested that the HIF signature observed initially after ICH may diminish over time (Figure 4A, Fig S8A). To evaluate HIF's transcriptional control of glycolytic metabolism in myeloid cells, we examined temporal shifts in expression of enzymes controlling each of the rate-limiting steps of glycolysis (Fig. 4B, Table S5). Glycolytic flux in mammalian cells is regulated by: 1) glucose import via GLUT3 and, to a lesser degree, GLUT1, 2) glucose phosphorylation by hexokinase II (*HK2*) (39, 40), 3) generation of fructose-1,6-biphosphate (F1,6-BP) by phosphofructokinase-1 (PFK-1), and 4) lactate export (39). PFK-1 activity is primarily controlled by PFK-2 (*PFKFB3*), which generates positive allosteric regulators of PFK-1 and thereby enhances glycolytic flux. Hematoma CD14+ monocytes/macrophages decreased expression of genes controlling each of these steps over time: expression of *SLC2A3* and *HK2* decreased four-fold and of *PFKFB3* by half during the acute stage of the response. *SLC2A1* showed a modest trend of decreased expression. Neutrophils also downregulated over time genes involved in glycolysis, with a four-fold reduction in *SLC2A3* expression and a 16-fold decrease in *HK2* expression (Fig. S8B). No change to expression of *SLC2A1* or *PFKFB3* was observed in neutrophils. All of these genes are targets of HIFs, and their coordinated downregulation during the acute stage suggested that HIF signaling in hematoma myeloid cells decreased over time from an initial peak early after ICH onset. Levels of lactate in the hematoma effluent decreased over the acute response to ICH (Fig. 4C), supporting the hypothesis that HIF-mediated augmentation of glycolytic metabolism in myeloid cells diminished over time after ICH.

Anabolic metabolism supported by aerobic glycolysis has been associated with inflammatory myeloid function, and treatment with glycolytic inhibitors suppresses inflammatory macrophage activation (16, 41, 42). Decreasing glycolytic flux over time after ICH could therefore represent a shift by myeloid cells away from inflammatory function and toward reparative programs. Over time, hematoma CD14+ monocytes/macrophages and neutrophils rapidly decreased expression of genes encoding inflammatory cytokines that had been highly expressed at the acute stage after ICH (Fig. 3), such as *IL6*, *IL1A*, and *CSF3* (Fig. 4D, S8C). Thus, after an initial burst of glycolysis and inflammatory cytokines gene expression by myeloid cells within the hematoma, their expression decreased over the first four days after hemorrhage.

Acquisition of a transcriptional program associated with repair is linked to metabolic reprogramming.

Decreased expression of glycolytic enzymes and inflammatory cytokines did not appear to represent a loss of activity by myeloid cells in the hematoma, but rather a shift in their functional programming. Gene ontology analysis of genes increased in expression over time after ICH (Fig. 1C) in hematoma CD14+ monocytes/macrophages and neutrophils revealed enrichment for phagocytosis, lysosome, and antigen presentation pathways (Fig. 5A, Fig. S9A), supporting a previously demonstrated role of these cells in clearance of erythrocytes

from the brain and neurological recovery in an animal model of ICH (6). CD14+ monocytes/macrophages, but not neutrophils, upregulated a suite of genes encoding phosphatidylserine receptors that mediate phagocytosis of apoptotic cells, including *MERTK*, *HAVCR2* (TIM-3), and *ITGAV* (αV integrin) (Fig. 5B, Fig. S9B). Both CD14+ monocytes/macrophages and neutrophils also increased expression over time of heme oxygenase (*HMOX1*, Fig. 5C, S9B), which catalyzes the degradation of heme and has anti-oxidative and anti-inflammatory functions (43).

While expression of glycolytic enzymes decreased in the hematoma during the transition from the acute to sub-acute stages of ICH, these genes were still significantly elevated compared to peripheral blood cells (Fig. 4B,C, Fig. S8B). Expression of *SLC7A5*, a cell surface transporter responsible for importing neutral amino acids to support leukocyte activation (44, 45), increased over time in both CD14+ monocytes/macrophages and neutrophils (Fig. 5C, Fig. S9C). Expression of *MYC*, which encodes c-Myc, a key transcription factor controlling anabolic metabolism (46), also increased over time in CD14+ monocytes/macrophages. These data suggest that although HIF-1 signaling and glycolytic gene expression decrease over time in myeloid cells within the hematoma, overall glycolysis, as well as the anabolic generation of proteins and lipids it supports, likely remains elevated in these cells throughout the observed time course.

Decreasing expression of inflammatory cytokines over time did not represent a universal downregulation of immune factors. Over the same period, expression of the monocyte chemoattractants *CCL2* and *CCL7* increased (Fig. 5D), potentially promoting continued monocyte recruitment to the injured CNS. Additionally, myeloid cells maintained expression of *PTGES* and *IL10* throughout the first week after ICH (Fig. 5E–F Fig. S9D–E). Macrophage-derived PGE_2 can suppress inflammatory microglial activation after spinal cord injury (47), increase neuronal resilience and augment neurogenesis after ICH (48), and guide astrocyte activation to support neurogenesis (49, 50). In summary, myeloid cells reprogrammed key functional pathways over time after ICH in conjunction with metabolic shifts, converting from primarily inflammatory activation states to states associated with repair and recovery.

The patients in our cohort received rtPA instilled into the hematoma after the first surgical aspiration, which raises the possibility that the longitudinal changes to myeloid cells we observed could be caused by rtPA exposure. rtPA-induced fibrinolysis could influence myeloid activation directly, via release of danger-associated molecular patterns (DAMP) from the clot, or due to hematoma drainage reducing oxidative or physical stressor signals. However, gene expression of cells isolated from hematoma effluent collected at the time of initial surgery, prior to rtPA administration, followed the same temporal trends as samples collected after rtPA exposure (Fig. S10), and *ex vivo* exposure of hematoma effluent to rtPA did not significantly affect expression of genes in the pathways highlighted in Figures 3, 4, or 5 (Table S8). Therefore, the observed changes in key myeloid gene expression over time within the hematoma were not likely caused by exposure to rtPA.

Increased glycolytic gene expression in CD14+ monocytes/macrophages is associated with good patient outcomes.

To examine the contribution of myeloid cells to neurological recovery in our patients, we performed differential gene expression analysis comparing myeloid gene expression at the sub-acute stage (>96 hours post-ICH), during which gene expression remained stable, in patients with good and poor outcomes as defined in the MISTIE III trial (18). Good outcome was defined as a modified Rankin score (mRS) of 0–3 (no disability to moderate disability) at one year post-ICH, while a poor outcome was defined as mRS score 4–6 (moderately severe disability to death). To account for clinical factors known to affect patient outcome after ICH, we incorporated the disease composite "severity index" from the MISTIE III parent trial (18) into the linear model used to determine differential gene expression. 17 patients contributed peripheral blood samples in this time range, while 15 contributed hematoma effluent samples.

This analysis revealed 561 significantly differentially expressed genes in hematoma CD14+ monocytes/macrophages during the sub-acute stage between patients with good and poor outcomes (Table S9). Hierarchical clustering of patients and genes revealed consistent patterns of gene expression within the good and poor outcome groups (Fig 6A), with the notable exception of a single patient with poor outcome resembling those with good outcomes. No unique clinical characteristics or events were observed for this patient, but the consistency of the gene expression patterns in the other patients suggests that their poor recovery may have been independent of the myeloid immune response. No differentially expressed genes were detected in neutrophils in the hematoma or blood, and just one differentially expressed gene (*TMEM51*, a trans-membrane protein of unknown function) was found in blood monocytes (Fig. S11). The strong association of outcome with a consistent transcriptional profile exclusively in hematoma CD14+ monocytes/macrophages suggests a potentially critical role for these cells in guiding neurological recovery after ICH.

Gene ontology (GO) analysis revealed strong enrichment for HIF-1α signaling and glycolysis pathways in hematoma CD14+ monocytes/macrophages from patients with good outcomes, while CD14+ monocytes/macrophages from patients with poor outcomes showed enrichment for oxidative glucose metabolism pathways (Fig. 6B, Table S10). Further analysis revealed that many of the genes in the metabolic and functional pathways initially identified in Figures 3, 4, and 5 were significantly correlated with outcome (Fig. 6C). Surprisingly, we did not detect significant differences in expression of most cytokines and chemokines between patients with good or poor outcomes, except for *IL24*, *CCL5*, and *CXCL5*, which were all more highly expressed in patients with good outcomes. Intriguingly, *PTGES* expression was increased more than 5-fold in patients with good outcome (BH adjusted $p = 0.0013$; Fig. 6D), indicating that myeloid-derived PGE_2 may contribute to neurological recovery in patients.

Hematoma CD14+ monocytes/macrophages from patients with good outcomes displayed higher expression of five key glycolytic enzymes during the sub-acute stage of the response: *HK2*, *ALDOA*, *GAPDH*, *PGAM1*, and *ENO2* (Fig. 6C,E, Table S9). *PFKM* expression was lower in patients with good outcomes, but its expression was also decreased in hematoma during the acute stage (Fig. 3) when glycolytic flux was at its highest, consistent with PFK

activity being generally controlled by PFK-2 in macrophages (39). Additionally, we saw decreased expression of seven enzymes in the TCA cycle in patients with good outcomes: *PDHA1*, *PDHB*, *IDH1*, *IDH2*, *SUCLG1*, *FH*, and *MDH1*. Thus, CD14+ monocytes/macrophages derived from patients with good outcomes appear to favor glycolysis over cellular respiration during the sub-acute stage of ICH, suggesting that glycolytic metabolism may have a previously unappreciated role in supporting reparative macrophage function. Patients with good outcome also displayed a trend towards higher levels of tissue lactate within the hematoma, after adjusting for initial disease severity (Fig. 6F). Although there are many potential cellular sources of lactate in the hematoma, this analysis further supported the transcriptional data that higher rates of glycolysis occur at the site of hemorrhage during the sub-acute stage of ICH in patients with good recovery.

HIF signaling and increased glycolysis are required for macrophage PGE_2 production.

Given the strong correlation of *PTGES* expression with good outcomes after ICH, we hypothesized that HIF-mediated glycolytic metabolism in macrophages contributed to functional recovery by supporting PGE_2 synthesis. To test this hypothesis, we stimulated monocyte-derived macrophages from healthy donors *in vitro* with a cocktail of ICH-associated danger signals (ICH-DAMP: IL-1β, S100A8, and thrombin, see Materials and Methods), finding that this stimulation induced secretion of many of the immune factors expressed by hematoma CD14+ monocytes/macrophages *in vivo* (Fig. 7, Fig. S12). ICH-DAMP stimulation drove increased expression of *HK2* by macrophages, as did the iron chelator deferoxamine (DFO), a positive control for HIF activation (Fig. 7A). This effect was HIF-dependent, as pre-treatment with the HIF inhibitor echinomycin blocked ICH-DAMP-mediated expression of *HK2* and increases in glycolytic flux (Fig. 7B).

ICH-DAMP stimulation also induced *PTGES* expression, and HIF signaling was necessary, but not sufficient, for this process (Fig. 7C). Indeed, inhibition of glycolysis, either directly with the glycolytic inhibitor 2-deoxyglucose (2-DG) or via HIF inhibition, not only suppressed macrophage secretion of the inflammatory cytokine IL-6 in response to stimulation with ICH-DAMP or IFN-γ + LPS, but also repressed production of the myeloid chemokines CCL2 and IL-8, and the anti-inflammatory effectors PGE_2 and IL-10 (Fig. 7D, Fig. S12). Thus, HIF-mediated aerobic glycolysis is not a specific feature of inflammatory macrophages, but rather may generally support anabolic metabolism and secretion of both pro- and anti-inflammatory factors by activated macrophages.

Monocyte-derived macrophages have previously been shown to resolve acute myeloid inflammation by inhibiting neutrophil recruitment and production of TNF and reactive oxygen species (ROS) via PGE_2 signaling (51, 52). PGE_2 can also act in an autocrine manner on macrophages to limit inflammatory factor production (53, 54). To examine whether PGE_2 could contribute to modulation of myeloid inflammatory responses and acquisition of reparative features, we stimulated human macrophages with ICH-DAMP in the presence or absence of exogenous PGE_2. Addition of exogenous PGE_2 diminished IL-6 production while augmenting production of VEGF (Fig 7E), which has been shown in mouse models to support angiongenesis and neurogenesis after acute brain injuries (55, 56).

These findings provide a potential mechanism by which glycolysis supports reparative macrophage responses via the production of pro-resolution mediators such as PGE_2.

Discussion

Here, we identify distinct stages of the early myeloid response to ICH within the hematoma that were highly conserved across our patient cohort. Our findings reveal coordinated functional and metabolic reprogramming in CD14+ monocytes/macrophages within the hematoma as they shift from inflammatory to reparative and anti-oxidative transcriptional states. Additionally, we report extensive metabolic reprogramming of neutrophils during acute neuroinflammation in patients. Interestingly, the profiles of monocytes and neutrophils in the peripheral blood were remarkably static during the time period of our study, suggesting that transcriptional analyses of these populations as a whole may not accurately reflect the dynamics of the immune response to brain injury.

Surprisingly, we find that expression of HIF target genes controlling glycolytic metabolism in macrophages is positively correlated with good neurological recovery after ICH. This stands in contrast with the prevailing view that glycolytic metabolism predominantly supports pro-inflammatory functions in macrophages (16, 36, 38, 57, 58). Notably, these studies have employed *in vitro* M1/M2 stimulation or highly polarized infection models in mice to assess the metabolic requirements for macrophage function. The metabolic requirements for inflammatory and reparative macrophage responses during sterile inflammation have remained largely unexplored, particularly in human patients (16). Our findings suggest that glycolytic metabolism in macrophages supports PGE_2 synthesis and therefore may contribute to recovery in patients after acute brain injury by inhibiting inflammatory cytokine production and augmenting production of VEGF. Macrophage-derived PGE_2 has previously been shown to enhance immune-mediated neurological recovery in animal models by dampening microglia and astrocyte activation. (50, 59–61). PGE_2 also enhances neuronal resilience to ferroptotic and inflammatory stress (48) and supports neurogenesis of many neuronal subtypes via direct signaling on neurons as well as indirectly by stimulating glutamate release from nearby astrocytes (49, 62–64). Further investigation is required to more clearly define the mechanistic underpinnings in macrophages connecting enhanced glycolysis, augmented PGE_2 synthesis, and improved neurological recovery after ICH.

The robust signatures associated with good and poor outcomes suggest that we were powered to detect critical transcriptional signals in CD14+ monocytes/macrophages after ICH. However, the lack of correlation between expression of other genes by hematoma CD14+ monocytes/macrophages may be a reflection of the number of patients in this study rather than evidence against their importance for neurological recovery. Furthermore, the switch from inflammatory to reparative activation states we observe over time in the hematoma may either reflect a functional switch by CD14+ monocytes/macrophages in this tissue throughout the measured timespan or the arrival of new cells from the periphery which acquire distinct functions according to the evolving hematoma milieu. Although our extensive profiling of the CD14+ population in the hematoma led us to conclude that these cells are predominantly derived from circulating CD14+ monocytes, the inclusion of a small

number of brain-resident microglia and border-associated macrophages into the sorted populations cannot be ruled out. In a case study of a single patient using the same surgical approach, single cell profiling did not uncover populations resembling brain-resident myeloid cells (65). Larger scale studies utilizing single-cell approaches as well as lineage tracing experiments could address this issue and may reveal whether myeloid populations in the hematoma are comprised of heterogeneous subsets of cells recruited during different stages of the response.

Overall, our study provides an analysis of the kinetics of activation of myeloid cells in the living human brain after acute injury, linking macrophage activation states and neurological patient outcomes. The strong glycolytic signature associated with recovery and the importance of glycolysis in supporting PGE_2 production by macrophages reported here highlight the importance of future studies on the metabolic underpinnings for reparative macrophage functions *in vivo*.

Materials and Methods

Study Design

The purpose of this study was to define distinct stages of myeloid responses in the peripheral blood and within the hematoma over time after ICH. Patient enrollment at approved study sites was performed according to the parent MISTIE III trial clinical trial (18). Hematoma effluent and peripheral blood samples were collected under the ICHseq sub-study trial until its conclusion. Samples from the first four enrolled patients were used to optimize cell isolation and sequencing techniques. All subsequent samples were included in the final dataset, yielding 82 blood monocyte samples, 57 hematoma macrophage samples, 76 blood neutrophil samples, and 49 hematoma neutrophil samples. 21 patients contributed CD14+ monocyte/macrophage samples that passed quality control filtering criteria (see Initial Data Processing); 17 patients contributed neutrophil samples. Peripheral blood myeloid cells from 5 age-matched healthy donors without ICH were analyzed in the same manner.

Whenever sufficient cell numbers allowed, technical replicates were produced by sorting additional pools of the same cells and generating cDNA libraries in parallel with all other samples. This resulted in technical replicates being included in the analysis for 19 blood monocyte profiles, 35 hematoma macrophage profiles, 10 blood neutrophil profiles, and 37 hematoma neutrophil profiles. Initial transcriptional analysis was performed blinded to tissue of origin, patient, and outcome. Outcome assessments were performed by blinded investigators as part of the parent MISTIE III trial, and then provided to the investigators of the ICHseq sub-study.

To interrogate the mechanistic underpinnings linking HIF activation, glycolysis, and macrophage function, human macrophages derived from healthy donor blood CD14+ monocytes were stimulated with ICH-DAMP in the presence or absence of the HIF inhibitor DFO, the glycolysis inhibitor 2-DG, or PGE_2. For these studies, experimental conditions were assessed in triplicate or greater for each individual donor, and 3–5 donors were used as biological replicates for each experiment.

Leukocyte Isolation

Leukocytes were isolated from blood and hematoma effluent using a protocol we developed previously of: 1) benzonase treatment to remove cell-free DNA and prevent clumping, 2) filtration to remove platelets and most erythrocytes, and 3) hypotonic lysis to eliminate remaining erythrocytes. This approach, unlike standard PBMC preparations, preserved neutrophils for downstream analysis. Samples were spun at 500*g* for 10 minutes. Supernatant (plasma or plasma equivalent) was removed and frozen at −80°C. This supernatant was later used to measure lactate and PGE_2 levels in the peripheral blood and hematoma effluent. The remaining cell layer was resuspended in Hank's balanced salt solution (HBSS) (Gibco #14170–112) and treated with 2.5 U/mL benzonase (Sigma #E1014) for 10 minutes at room temperature. Samples were subsequently filtered (70 micron), washed with 25 mL of HBSS, and centrifuged at 300*g* for 8 minutes. After supernatants were removed, platelets and most erythrocytes were removed from these samples using a LeukoLock filter (included in Life Technologies #AM1933) as previously described (66). Briefly, samples were resuspended in HBSS and passed through pre-washed LeukoLock filters by gravity (aided by flushing with a transfer pipette if flow via gravity was impeded). The filter was then rinsed with 3 mL of HBSS, then backflushed with 20 mL HBSS to recapture the leukocytes bound from the filter. After centrifugation, supernatants were removed and samples were treated with erythrocyte lysis buffer (BD #555899) for 15 minutes at room temperature, washed with 25 mL of HBSS, centrifuged at 300*g* for 8 minutes, and resuspended in X-VIVO 15 (Lonza #04–418Q) for cell counting.

Cell cover fixation, magnetic separation, and FACS-sorting of samples

Up to 5×10^6 leukocytes isolated from each sample were used for downstream sorting. Cells were first fixed in 1 mL of Cell Cover, a light preservative that maintains RNA integrity (Anacyte #800–250), on ice for 10 minutes, then centrifuged. $CD3^+$ cells were removed from total cell suspensions by magnetic selection (StemCell #17851) according to manufacturer's instructions. CD3- fractions were incubated on ice for 12 minutes in PBS supplemented with 0.5% FBS (Gibco #16140–071) using the following antibodies: CD45 (HI30, Tonbo Biosciences #50–0459-T100), CD11b (ICRF44, Tonbo #35–0118-T100), CD14 (M5E2, Biolegend #301820), CD16 (3G8, BD #560474), CD66a/c/e (ASL-32, Biolegend #342310), CD2, (RPA-2.10, Biolegend #300204), CD20 (2H7, Biolegend #302349), CD56 (HCD56, Biolegend #318320), and viability dye (Life Technologies, #L34972). After washing out the antibody stain with HBSS, samples were stained for 20 minutes on ice with viability dye diluted in HBSS (Life Technologies #L34972). Cells were resuspended in PBS plus 0.5% FBS and myeloid populations were sorted using a FACSaria II (Fig. S2) directly into RNA lysis buffer composed of 200 μL RA1 buffer (Macherey-Nagel #RA1) freshly spiked with 2% TCEP (Thermofisher #77720).

RNA isolation & cDNA library generation

RNA-sequencing libraries were generated as previously described (66, 67). Briefly, RNA was extracted using the NucleoSpin RNA XS Kit (Macherey-Nagel #740902) according to the manufacturer's instructions. Smart-Seq2 cDNA synthesis was performed as described by Picelli et al (67) with the following modifications: 1) input RNA was normalized prior to

cDNA generation by diluting to ~1,000 cells per reaction, 2) reverse transcription was performed with Superscript III (ThermoFisher #18080–085) in place of Superscript II according to the manufacturer instructions. Paired-end sequencing libraries were prepared using the Nextera XT DNA sample Prep Kit (Illumina #FC-131) according to the manufacturer's instructions.

Sequencing & alignment

Libraries were pooled in an equimolar ratio and sequenced on a NextSeq500 sequencer (Illumina) using a 75 cycle v2 sequencing kit with a paired end read structure. Following sequencing, BAM files were converted to merged, demultiplexed FASTQs. Paired-end reads were mapped to the UCSC hg19 genome using STAR and RSEM.

Initial data processing

Aligned expression matrices generated by STAR were first filtered based on read depth and captured gene depth to remove low quality samples. A minimum of 4×10^6 FASTQ fragments and a minimum of 9,000 (for CD14+ monocytes/macrophages) or 8,500 (for neutrophils) captured genes were used as inclusion criteria. Samples lacking patient metadata or occurring later than 171h post-ICH were excluded, removing two additional samples for each cell type. Genes with fewer than 1 count per million (CPM) in greater than 80% of the samples of a given cell type were considered unexpressed and filtered out prior to downstream analysis. Filtered counts matrices with technical replicates included were used as input for differential expression (see below). For data visualization (PCAs, gene expression scatter plots, and gene expression plots), filtered counts from technical replicates were collapsed together using the "edgeR" pipeline. Trimmed mean of M (TMM) values library size normalization (68) was used to account for differences in sequenced reads between samples. Normalized library sizes were used for frequency estimation in generation of log-FPKM matrices.

Principal component analysis (PCA)

Prior to PCA, batch correction was performed using the "removeBatchEffect" command in the "limma" gene expression analysis package for R (25). Batch effects were predominantly related to levels of ribosomal gene expression; genes of interest did not demonstrate noticeable batch effects (Table S11). PCA was performed without scaling unit variance and plotted using the "ggbiplot" package for R; results were similar if scaling was performed prior to plotting.

Myeloid Activation ssGSEA

ssGSEA was performed with the same parameters as above. Statistical significance was determined by two-tailed student's *t*-test corrected for multiple comparisons by the Benjamini-Hochberg method because enrichment scores were normally distributed across all samples.

Differential gene expression analysis

Differential gene expression analysis was performed using generalized linear modeling with the limma package for R using the “limma-voom” methodology (25, 26, 69). For all analyses, peripheral blood cells and hematoma cells were analyzed together using a single model, with the origin tissue of the cells included as a parameter in the design matrix. For certain analyses, additional parameters and/or interaction terms were included in the linear model, as noted in the text and/or figure legends. Batch correction was not performed prior to differential expression; rather, empirically determined sample weights were used to down-weight lower quality samples using the “voomWithQualityWeights” command in the limma package. This decreased the weight of samples with higher proportions of ribosomal RNA. This approach was employed because patient samples were not randomly distributed across all batches; all samples from a particular patient were sequenced within a single batch in order to study within-patient changes over time. Batch correction would therefore have improperly reduced patient-to-patient variation prior to differential gene expression. Differentially expressed genes in all analyses were determined using the empirical Bayes method with a significance threshold set at a Benjamini-Hochberg (BH) adjusted p value of 0.05; no fold-change threshold was used. The conclusions of these analyses were robust against altering parameters for determining significance (for example introducing a fold-change threshold or lowering the p value threshold).

Spline regression and k-means clustering of gene expression changes over time

To determine genes changing significantly over time in hematoma and blood, a cubic spline basis with 2 degrees of freedom (1 knot) was formed to fit each gene’s expression level against time using the “splines” package in R. This spline basis was input as an interacting term with the tissue compartment in the design matrix of the linear model, so that a separate spline was fit to samples from the blood and hematoma compartments for each gene evaluated (Fig. S5). Genes with significant fits to the hematoma regression spline (BH adjusted $p < 0.05$) were first filtered to remove genes with no expression in hematoma samples, then spline fits were clustered by k means to find modules of genes with shared patterns of change over time (Fig. S5A, E). Gene fits using splines with 2 or more knots were also assessed, but this approach did not provide superior results. The number of clusters was determined by the “elbow” of a total within clusters sum of squares plot. Optimal initial means for generating stable clusters were determined by iterating 1,000 initial starting values and selecting values that both gave clusters with high stability across all iterations and minimized the within cluster sum of squares distance. No batch correction was performed prior to spline regression or visualization.

For the graphical representations of the cubic spline regression models of changes over time in the hematoma (Fig. 1C, Fig. S5), the y axis depicts the change from the gene expression in the earliest collected hematoma sample. Log2 gene expression levels of each gene in every hematoma sample were normalized to that observed in the earliest sample (37h post-ICH) by subtracting the gene expression value in the 37h sample from every sample.

Differential gene expression of blood versus hematoma at acute stage

To determine differentially expressed genes between tissues during the acute stage of ICH, a separate linear model was built using the limma package for each cell type with tissue compartment as the only parameter. Only the first blood and first hematoma effluent sample from each patient was included in the analysis; these samples ranged from 23–99 hours post-ICH (Tables S1, S2). Technical replicates were included by estimating their correlation and blocking for them in the linear model according to the methods described in the limma user's guide (69).

Differential gene expression according to patient outcome

To determine differentially expressed genes according to patient outcome at 365 days post-ICH, modified Rankin scores (mRS) calculated by the MISTIE III clinical trial were dichotomized to either "good" (mRS 0–3), or "poor" (mRS 4–6) outcomes. Samples were included only from the sub-acute stage of the ICH response when gene expression was temporally stable (>96 hours post-ICH). 15 patients from our initial cohort of 21 contributed hematoma effluent samples during this time range, the other 6 patients in our cohort contributed samples only during the acute stage and were therefore excluded from this analysis. Differential expression analysis on outcome was adjusted for initial disease severity using a composite severity score defined by the MISTIE III trial (18). The severity score incorporated patient age, initial Glasgow coma score, pre-existing white matter disease and diabetes status, location of the hemorrhage, hemorrhage volume, and intraventricular volume. This analysis included repeated measures from the same patients; both technical replication and biological replication were accounted for in a two-step process. First, gene expression from technical replicates were collapsed together using the edgeR package, generating a single sample from each patient at a particular timepoint. Second, repeated measures from the same patient collected on different days >96 hours post-ICH were considered biological replicates because gene expression was static in this time range (Fig. 1C) and accounted for by estimating their correlation and blocking for them in the linear model as a random effect.

Lactate and PGE_2 measurements

Cell-free supernatants were isolated from peripheral blood and hematoma effluent as described in the "Leukocyte isolation" section of the methods. Supernatants were then centrifuged at 2000*g* for 10 minutes to remove cellular debris; supernatant was aliquoted and frozen at −80°C. Lactate levels were measured using the Lactate Colorimetric Assay Kit II (Biovision #K627) according to the manufacturer's instructions. PGE_2 was measured both *ex vivo* supernatants as well as macrophage culture supernatants using the Prostaglandin E2 monoclonal ELISA kit (Cayman Chemical #514010) according to the manufacturer's instructions. All samples were run in duplicate and the average of the two replicates was taken as the final measurement. Samples that were above the dynamic range of the assays were diluted in PBS (*ex vivo* sample supernatants), or cell culture medium (macrophage culture supernatants), and re-run to obtain accurate measurements.

Statistical analysis of changes to tissue lactate levels over time

To determine whether lactate levels changed significantly over time in the hematoma and blood, a cubic spline with 2 degrees of freedom (1 knot) was fitted to the measured lactate levels over time after ICH. This spline was used as an interacting term with the tissue compartment in the design matrix of a linear model (akin to the approach used for differential gene expression over time), so that a separate spline was fit to samples from the blood and hematoma compartments. F tests were performed to determine the significance of the spline regressor in the linear model assess whether the level of lactate changed significantly over time.

Statistical analysis of lactate levels stratified by outcome

Only lactate measurements from hematoma samples collected during the sub-acute stage (>96 hours post-ICH) were included in this analysis because lactate levels were determined to be stable after this point. Repeated measures from the same patient collected on different days >96 hours post-ICH were therefore considered biological replicates; the mean lactate from all replicates was used to calculate each patient's individual lactate level during the time period. Statistical comparison of lactate by outcome was adjusted for initial disease severity using a composite severity score defined by the MISTIE III trial (18), as described above for differential gene expression stratified by outcome. Severity score and mean lactate levels for each patient were entered as parameters in a linear model and a F test was performed to determine the significance of correlation between lactate level and outcome.

Human monocyte-derived macrophage cultures

Peripheral blood mononuclear cells (PBMCs) were isolated from blood collected from healthy donors (median age 64 years (IQR 60–71, 50% male) over a Ficoll-Paque Premium gradient (GE Healthcare #17544203). CD14+ monocytes were purified from PBMCs by magnetic cell separation using the EasySep Human CD14 Positive Selection Kit II (STEMCELL Technologies #17858). Monocytes were seeded in tissue culture treated plates at the following densities: 250,000 cells/well in 24 well plates (Corning #353407), used for qPCR measurements, 125,000 cells/well in Seahorse XF96 microplates (Agilent #101085–004) for measurements of glycolytic flux, and 35,000 cells/well in 96 well plates (Corning #3599) used for cytokine and PGE_2 measurements. Cells were cultured in RPMI 1640 medium (Gibco #11875–903) supplemented with 100 ng/ml M-CSF (Tonbo #21–8789-U100), 10% FBS (Gibco #16140–071), 20 mM HEPES (Gibco #15630–080), 1 mM sodium pyruvate (Gibco #11360–070), non-essential amino acids (Gibco #11140–050), 100 U/mL penicillin/streptomycin (Gibco, #15140–122), and 2 mM L-glutamine (Gibco #25030–081) for 7 days; macrophages were used between day 8 and 10 of culture. Cell culture medium was completely refreshed at days 3 and 6.

Macrophage stimulation with ICH-DAMP

Intracerebral hemorrhage results in the release of DAMP at the site of hemorrhage that contribute to the subsequent localized inflammatory response within the brain. Previous work has established thrombin-PAR1 signaling as a key pathway for driving this process *in vivo* (2), but other factors remain unexplored. IPA upstream regulator analysis revealed

S100A8 (activation Z score = 2.52, $p<0.001$) and IL-1β (activation Z score = 4.41, $p<0.001$) as additional potential soluble factors for mediating gene expression changes in hematoma CD14+ monocytes/macrophages compared to peripheral cells. Therefore, to model macrophage activation after ICH in an *ex vivo* setting, monocyte-derived macrophages from healthy donors were stimulated with S100A8 (1 μg/mL, Biolegend #719908), endotoxin free thrombin (10 U/mL, Sigma #T1063–1KU), and IL-1β (10 ng/mL, Biolegend #579402). This stimulation paradigm resulted in cytokine secretion patterns that resembled those seen after stimulation with LPS + IFN-γ, as well as macrophage cytokine transcript levels observed *in vivo* after ICH (Fig. 3, 7, S12).

qPCR

Healthy donor monocyte-derived macrophages were pre-treated with 50 nM echinomycin (Sigma #SML0477) or vehicle control (0.1% DMSO) in fresh culture medium for 1 hour prior to treatment with 100 μg/mL deferoxamine (Sigma #D9533), ICH-DAMP cocktail, or vehicle control (water), with two replicate wells per condition. After 8 hours of treatment, cells were lysed using Qiazol (Qiagen #79306) and RNA was isolated using the miRNeasy micro kit (Qiagen #217084). cDNA was generated using the SuperScript VILO cDNA Synthesis Kit (Thermofisher #11756500). Because *GADPH* and *ACTB* were differentially expressed by myeloid cells after ICH (Tables S4, S5, S9), *PSMB2* was used as a housekeeping gene, as previously reported (70). Taqman primers were used to estimate expression of *PSMB2* (Thermofisher #Hs01002946_m1), *PTGES* (#Hs01115610_m1), and *HK2* (#Hs00606086_m1). Statistical significance between was determined using two-way ANOVA with Dunnett's correction for multiple comparisons.

Glycolytic flux analysis

For experiments measuring glycolytic flux, on day 8 of culture, macrophage media was replaced with "Seahorse medium": Glucose-free DMEM supplemented with M-CSF (100 ng/ml, Tonbo #21–8789-U100), FBS (Gibco #16140–071), glucose (11 mM, Sigma #G8270), L-glutamine (2 mM, Sigma #G3126), and HEPES (10 mM, American Bio #AB06021–00100). Healthy donor monocyte-derived macrophages plated in Seahorse XF96 microplates were washed twice with Seahorse medium and then incubated in Seahorse medium at 37°C in a non-CO_2 injected incubator. Extracellular acidification rates were measured by an XFe96 analyzer (Agilent) according to manufacturer's protocols with 5 replicates per condition. Readings for each well were normalized according to the baseline extracellular acidification rate (ECAR) reading prior to stimulation, as recommended by the manufacturer. Statistical significance was determined by repeated measures two-way ANOVA.

Metabolic inhibition of macrophage stimulation

Healthy donor monocyte-derived macrophages were pre-treated with varying doses of echinomycin (Sigma #SML0477) or vehicle control (0.1% DMSO) in fresh culture medium for 1 hour prior to treatment with deferoxamine (100 μg/mL, Sigma #D9533), ICH-DAMP cocktail, or vehicle control (water). After 24 hours of treatment, cell supernatants were collected and frozen at −80°C for subsequent analysis, with 5 replicate wells per condition.

Statistical significance was determined by one-way ANOVA with Dunnet's correction for multiple comparisons.

PGE_2 inhibition of macrophage stimulation

Healthy donor monocyte-derived macrophages were stimulated with ICH-DAMP cocktail in the presence or absence of 100 nM PGE_2 (Cayman chemical #14010), or vehicle control (PBS). After 48 hours of treatment, cell supernatants were collected and frozen at −80°C for subsequent analysis, with 5 replicate wells per condition. Statistical significance was determined by paired ratio student's *t*-tests between conditions.

Cytokine measurements

IL-6, IL-10, CCL2, IL-8, IL-10, and VEGF were measured by cytokine bead array (BD #558264) according to the manufacturer's instructions. Measurements for CCL2 and IL-8 were above the dynamic range of the assays; for these measurements, samples were diluted 20-fold in cell culture medium prior to analysis to obtain accurate measurements. Statistical significance was determined using one-way ANOVA with Dunnett's correction for multiple comparisons.

Supplementary Material

Refer to Web version on PubMed Central for supplementary material.

Acknowledgments

We thank the patients and families for their participation in ICH-seq, without whom this study would not have been possible. Clinical coordinators at participating sites worked tirelessly to collect and ship the samples used for this study. Additional appreciation to Lesley Devine, Chao Wang, and Khadir Raddassi for their assistance in cell sorting, and to Duanduan Ma, Kelson Zawack, Jonathan Delong, and Jenna Pappalardo for consultation and advice on transcriptional analysis.

Funding

Support for this research was provided by ICHseq (R01NS097728, PI Sansing), MISTIE III (U01NS080824, PI Hanley), NRSA postdoctoral fellowship (F32-AI136459, Goods), AHA postdoctoral fellowship (17POST33660872, Askenase), the Searle Scholars Program (Shalek), the Beckman Young Investigator Program (Shalek), a Sloan Fellowship in Chemistry (Shalek), and NIH 5U24AI118672 (PI Shalek). Recombinant human rtPA for the *in vitro* experiments was provided by Genentech.

Data and materials availability

The sequencing data for this study have been deposited in the database Gene Expression Omnibus (GEO) under the accession number GSE163256. The data can be explored interactively at https://ichseq.sansinglab.research.yale.edu, including comparing individual genes across time and patient outcomes. All other data needed to evaluate the conclusions in the paper are present in the paper or the Supplementary Materials.

References

1. Jassam YN, Izzy S, Whalen M, McGavern DB, El Khoury J, Neuroimmunology of Traumatic Brain Injury: Time for a Paradigm Shift, Neuron 95, 1246–1265 (2017). [PubMed: 28910616]

2. Keep RF, Hua Y, Xi G, Intracerebral haemorrhage: mechanisms of injury and therapeutic targets, The Lancet Neurology 11, 720–731 (2012). [PubMed: 22698888]

3. Russo MV, Latour LL, McGavern DB, Distinct myeloid cell subsets promote meningeal remodeling and vascular repair after mild traumatic brain injury, Nat Immunol 19, 442–452 (2018). [PubMed: 29662169]

4. Zhao X, Ting S-M, Sun G, Roy-O'Reilly M, Mobley AS, Bautista Garrido J, Zheng X, Obertas L, Jung JE, Kruzel M, Aronowski J, Beneficial Role of Neutrophils Through Function of Lactoferrin After Intracerebral Hemorrhage, Stroke 49, 1241–1247 (2018). [PubMed: 29636422]

5. Wattananit S, Tornero D, Graubardt N, Memanishvili T, Monni E, Tatarishvili J, Miskinyte G, Ge R, Ahlenius H, Lindvall O, Schwartz M, Kokaia Z, Monocyte-Derived Macrophages Contribute to Spontaneous Long-Term Functional Recovery after Stroke in Mice, J. Neurosci. 36, 4182–4195 (2016). [PubMed: 27076418]

6. Chang C-F, Goods BA, Askenase MH, Hammond MD, Renfroe SC, Steinschneider AF, Landreneau MJ, Ai Y, Beatty HE, da Costa LHA, Mack M, Sheth KN, Greer DM, Huttner A, Coman D, Hyder F, Ghosh S, Rothlin CV, Love JC, Sansing LH, Erythrocyte efferocytosis modulates macrophages towards recovery after intracerebral hemorrhage, J Clin Invest 128, 607–624 (2018). [PubMed: 29251628]

7. Kim CC, Nakamura MC, Hsieh CL, Brain trauma elicits non-canonical macrophage activation states, Journal of Neuroinflammation 13, 117 (2016). [PubMed: 27220367]

8. Martinez FO, Gordon S, The M1 and M2 paradigm of macrophage activation: time for reassessment, F1000Prime Rep 6, 13 (2014). [PubMed: 24669294]

9. Gordon S, Plüddemann A, Martinez Estrada F, Macrophage heterogeneity in tissues: phenotypic diversity and functions, Immunol Rev 262, 36–55 (2014). [PubMed: 25319326]

10. Mosser DM, Edwards JP, Exploring the full spectrum of macrophage activation, Nat Rev Immunol 8, 958–969 (2008). [PubMed: 19029990]

11. Phillipson M, Kubes P, The Healing Power of Neutrophils, Trends Immunol 40, 635–647 (2019). [PubMed: 31160208]

12. Jha AK, Huang SC-C, Sergushichev A, Lampropoulou V, Ivanova Y, Loginicheva E, Chmielewski K, Stewart KM, Ashall J, Everts B, Pearce EJ, Driggers EM, Artyomov MN, Network integration of parallel metabolic and transcriptional data reveals metabolic modules that regulate macrophage polarization, Immunity 42, 419–430 (2015). [PubMed: 25786174]

13. Xue J, Schmidt SV, Sander J, Draffehn A, Krebs W, Quester I, De Nardo D, Gohel TD, Emde M, Schmidleithner L, Ganesan H, Nino-Castro A, Mallmann MR, Labzin L, Theis H, Kraut M, Beyer M, Latz E, Freeman TC, Ulas T, Schultze JL, Transcriptome-based network analysis reveals a spectrum model of human macrophage activation, Immunity 40, 274–288 (2014). [PubMed: 24530056]

14. Cheng S-C, Quintin J, Cramer RA, Shepardson KM, Saeed S, Kumar V, Giamarellos-Bourboulis EJ, Martens JHA, Rao NA, Aghajanirefah A, Manjeri GR, Li Y, Ifrim DC, Arts RJW, van der Veer BMJW, van der Meer BMJW, Deen PMT, Logie C, O'Neill LA, Willems P, van de Veerdonk FL, van der Meer JWM, Ng A, Joosten LAB, Wijmenga C, Stunnenberg HG, Xavier RJ, Netea MG, mTOR- and HIF-1α-mediated aerobic glycolysis as metabolic basis for trained immunity, Science 345, 1250684–1250684 (2014). [PubMed: 25258083]

15. Cheng S-C, Scicluna BP, Arts RJW, Gresnigt MS, Lachmandas E, Giamarellos-Bourboulis EJ, Kox M, Manjeri GR, Wagenaars JAL, Cremer OL, Leentjens J, van der Meer AJ, van de Veerdonk FL, Bonten MJ, Schultz MJ, Willems PHGM, Pickkers P, Joosten LAB, van der Poll T, Netea MG, Broad defects in the energy metabolism of leukocytes underlie immunoparalysis in sepsis, Nat Immunol 17, 406–413 (2016). [PubMed: 26950237]

16. Van den Bossche J, O'Neill LA, Menon D, Macrophage Immunometabolism: Where Are We (Going)? Trends Immunol 38, 395–406 (2017). [PubMed: 28396078]

17. Artyomov MN, Sergushichev A, Schilling JD, Integrating immunometabolism and macrophage diversity, Semin. Immunol. 28, 417–424 (2016). [PubMed: 27771140]

18. Hanley DF, Thompson RE, Rosenblum M, Yenokyan G, Lane K, McBee N, Mayo SW, Bistran-Hall AJ, Gandhi D, Mould WA, Ullman N, Ali H, Carhuapoma JR, Kase CS, Lees KR, Dawson J, Wilson A, Betz JF, Sugar EA, Hao Y, Avadhani R, Caron J-L, Harrigan MR, Carlson AP, Bulters

D, LeDoux D, Huang J, Cobb C, Gupta G, Kitagawa R, Chicoine MR, Patel H, Dodd R, Camarata PJ, Wolfe S, Stadnik A, Money PL, Mitchell P, Sarabia R, Harnof S, Barzo P, Unterberg A, Teitelbaum JS, Wang W, Anderson CS, Mendelow AD, Gregson B, Janis S, Vespa P, Ziai W, Zuccarello M, Awad IA, MISTIE III Investigators, Efficacy and safety of minimally invasive surgery with thrombolysis in intracerebral haemorrhage evacuation (MISTIE III): a randomised, controlled, open-label, blinded endpoint phase 3 trial, Lancet 393, 1021–1032 (2019). [PubMed: 30739747]

19. Villani A-C, Satija R, Reynolds G, Sarkizova S, Shekhar K, Fletcher J, Griesbeck M, Butler A, Zheng S, Lazo S, Jardine L, Dixon D, Stephenson E, Nilsson E, Grundberg I, McDonald D, Filby A, Li W, De Jager PL, Rozenblatt-Rosen O, Lane AA, Haniffa M, Regev A, Hacohen N, Single-cell RNA-seq reveals new types of human blood dendritic cells, monocytes, and progenitors, Science 356 (2017), doi:10.1126/science.aah4573.
20. Gosselin D, Skola D, Coufal NG, Holtman IR, Schlachetzki JCM, Sajti E, Jaeger BN, O'Connor C, Fitzpatrick C, Pasillas MP, Pena M, Adair A, Gonda DD, Levy ML, Ransohoff RM, Gage FH, Glass CK, An environment-dependent transcriptional network specifies human microglia identity, Science 356, eaal3222 (2017). [PubMed: 28546318]
21. van der Poel M, Ulas T, Mizee MR, Hsiao C-C, Miedema SSM, Adelia, Schuurman KG, Helder B, Tas SW, Schultze JL, Hamann J, Huitinga I, Transcriptional profiling of human microglia reveals grey-white matter heterogeneity and multiple sclerosis-associated changes, Nat Commun 10, 1139–13 (2019). [PubMed: 30867424]
22. Gautier EL, Shay T, Miller J, Greter M, Jakubzick C, Ivanov S, Helft J, Chow A, Elpek KG, Gordonov S, Mazloom AR, Ma'ayan A, Chua W-J, Hansen TH, Turley SJ, Merad M, Randolph GJ, Immunological Genome Consortium, Gene-expression profiles and transcriptional regulatory pathways that underlie the identity and diversity of mouse tissue macrophages, Nat Immunol 13, 1118–1128 (2012). [PubMed: 23023392]
23. Van Hove H, Martens L, Scheyltjens I, De Vlaminck K, Pombo Antunes AR, De Prijck S, Vandamme N, De Schepper S, Van Isterdael G, Scott CL, Aerts J, Berx G, Boeckxstaens GE, Vandenbroucke RE, Vereecke L, Moechars D, Guilliams M, van Ginderachter JA, Saeys Y, Movahedi K, A single-cell atlas of mouse brain macrophages reveals unique transcriptional identities shaped by ontogeny and tissue environment, Nat Neuro 22, 1021–1035 (2019).
24. Goldmann T, Wieghofer P, Jordão MJC, Prutek F, Hagemeyer N, Frenzel K, Amann L, Staszewski O, Kierdorf K, Krueger M, Locatelli G, Hochgerner H, Zeiser R, Epelman S, Geissmann F, Priller J, Rossi FMV, Bechmann I, Kerschensteiner M, Linnarsson S, Jung S, Prinz M, Origin, fate and dynamics of macrophages at central nervous system interfaces, Nat Immunol 17, 797–805 (2016). [PubMed: 27135602]
25. Ritchie ME, Phipson B, Wu D, Hu Y, Law CW, Shi W, Smyth GK, limma powers differential expression analyses for RNA-sequencing and microarray studies, Nucleic Acids Res. 43, e47 (2015). [PubMed: 25605792]
26. Law CW, Chen Y, Shi W, Smyth GK, voom: Precision weights unlock linear model analysis tools for RNA-seq read counts, 15, R29 (2014).
27. Liberzon A, Birger C, Thorvaldsdóttir H, Ghandi M, Mesirov JP, Tamayo P, The Molecular Signatures Database (MSigDB) hallmark gene set collection, Cell Syst 1, 417–425 (2015). [PubMed: 26771021]
28. Bohlen CJ, Bennett FC, Tucker AF, Collins HY, Mulinyawe SB, Barres BA, Diverse Requirements for Microglial Survival, Specification, and Function Revealed by Defined-Medium Cultures, Neuron 94, 759–773.e8 (2017). [PubMed: 28521131]
29. Farhadian SF, Mehta SS, Zografou C, Robertson K, Price RW, Pappalardo J, Chiarella J, Hafler DA, Spudich SS, Single-cell RNA sequencing reveals microglia-like cells in cerebrospinal fluid during virologically suppressed HIV, JCI Insight 3 (2018), doi:10.1172/jci.insight.121718.
30. Sergushichev AA, Loboda AA, Jha AK, Vincent EE, Driggers EM, Jones RG, Pearce EJ, Artyomov MN, GAM: a web-service for integrated transcriptional and metabolic network analysis, Nucleic Acids Res. 44, W194–200 (2016). [PubMed: 27098040]
31. Baardman J, Verberk SGS, Prange KHM, van Weeghel M, van der Velden S, Ryan DG, Wüst RCI, Neele AE, Speijer D, Denis SW, Witte ME, Houtkooper RH, O'Neill LA, Knatko EV, Dinkova-Kostova AT, Lutgens E, de Winther MPJ, Van den Bossche J, A Defective Pentose Phosphate

Pathway Reduces Inflammatory Macrophage Responses during Hypercholesterolemia, Cell Rep 25, 2044–2052.e5 (2018). [PubMed: 30463003]

32. Düvel K, Yecies JL, Menon S, Raman P, Lipovsky AI, Souza AL, Triantafellow E, Ma Q, Gorski R, Cleaver S, Vander Heiden MG, MacKeigan JP, Finan PM, Clish CB, Murphy LO, Manning BD, Activation of a metabolic gene regulatory network downstream of mTOR complex 1, Mol. Cell 39, 171–183 (2010). [PubMed: 20670887]
33. O'Neill LAJ, Kishton RJ, Rathmell J, A guide to immunometabolism for immunologists, Nat Rev Immunol 16, 553–565 (2016). [PubMed: 27396447]
34. Hamidi T, Cano CE, Grasso D, Garcia MN, Sandi MJ, Calvo EL, Dagorn J-C, Lomberk G, Urrutia R, Goruppi S, Carracedo A, Velasco G, Iovanna JL, Nupr1-aurora kinase A pathway provides protection against metabolic stress-mediated autophagic-associated cell death, Clin. Cancer Res. 18, 5234–5246 (2012). [PubMed: 22899799]
35. Barbosa-Sampaio HC, Drynda R, Liu B, Rodriguez De Ledesma AM, Malicet C, Iovanna JL, Jones PM, Muller DS, Persaud SJ, Reduced nuclear protein 1 expression improves insulin sensitivity and protects against diet-induced glucose intolerance through up-regulation of heat shock protein 70, Biochim. Biophys. Acta 1852, 962–969 (2015). [PubMed: 25638293]
36. Cramer T, Yamanishi Y, Clausen BE, Förster I, Pawlinski R, Mackman N, Haase VH, Jaenisch R, Corr M, Nizet V, Firestein GS, Gerber HP, Ferrara N, Johnson RS, HIF-1alpha is essential for myeloid cell-mediated inflammation, Cell 112, 645–657 (2003). [PubMed: 12628185]
37. Peyssonnaux C, Datta V, Cramer T, Doedens A, Theodorakis EA, Gallo RL, Hurtado-Ziola N, Nizet V, Johnson RS, HIF-1alpha expression regulates the bactericidal capacity of phagocytes, Journal of Clinical Investigation 115, 1806–1815 (2005).
38. Corcoran SE, O'Neill LAJ, HIF1α and metabolic reprogramming in inflammation, J Clin Invest 126, 3699–3707 (2016). [PubMed: 27571407]
39. Tanner LB, Goglia AG, Wei MH, Sehgal T, Parsons LR, Park JO, White E, Toettcher JE, Rabinowitz JD, Four Key Steps Control Glycolytic Flux in Mammalian Cells, Cell Syst 7, 49–62.e8 (2018). [PubMed: 29960885]
40. Everts B, Amiel E, van der Windt GJW, Freitas TC, Chott R, Yarasheski KE, Pearce EL, Pearce EJ, Commitment to glycolysis sustains survival of NO-producing inflammatory dendritic cells, Blood 120, 1422–1431 (2012). [PubMed: 22786879]
41. Everts B, Amiel E, Huang SC-C, Smith AM, Chang C-H, Lam WY, Redmann V, Freitas TC, Blagih J, van der Windt GJW, Artyomov MN, Jones RG, Pearce EL, Pearce EJ, TLR-driven early glycolytic reprogramming via the kinases TBK1-IKKε supports the anabolic demands of dendritic cell activation, Nat Immunol 15, 323–332 (2014). [PubMed: 24562310]
42. Tannahill GM, Curtis AM, Adamik J, Palsson-McDermott EM, McGettrick AF, Goel G, Frezza C, Bernard NJ, Kelly B, Foley NH, Zheng L, Gardet A, Tong Z, Jany SS, Corr SC, Haneklaus M, Caffrey BE, Pierce K, Walmsley S, Beasley FC, Cummins E, Nizet V, Whyte M, Taylor CT, Lin H, Masters SL, Gottlieb E, Kelly VP, Clish C, Auron PE, Xavier RJ, O'Neill LAJ, Succinate is an inflammatory signal that induces IL-1β through HIF-1α, Nature 496, 238–242 (2013). [PubMed: 23535595]
43. Gozzelino R, Jeney V, Soares MP, Mechanisms of Cell Protection by Heme Oxygenase-1, Annu. Rev. Pharmacol. Toxicol. 50, 323–354 (2010). [PubMed: 20055707]
44. Yoon BR, Oh Y-J, Kang SW, Lee EB, Lee W-W, Role of SLC7A5 in Metabolic Reprogramming of Human Monocyte/Macrophage Immune Responses, Front Immun 9, 53 (2018).
45. Sinclair LV, Rolf J, Emslie E, Shi Y-B, Taylor PM, Cantrell DA, Control of amino-acid transport by antigen receptors coordinates the metabolic reprogramming essential for T cell differentiation, Nat Immunol 14, 500–508 (2013). [PubMed: 23525088]
46. Dejure FR, Eilers M, MYC and tumor metabolism: chicken and egg, EMBO J 36, 3409–3420 (2017). [PubMed: 29127156]
47. Greenhalgh AD, Zarruk JG, Healy LM, Baskar Jesudasan SJ, Jhelum P, Salmon CK, Formanek A, Russo MV, Antel JP, McGavern DB, McColl BW, David S, Peripherally derived macrophages modulate microglial function to reduce inflammation after CNS injury, PLoS Biol. 16, e2005264 (2018). [PubMed: 30332405]

48. Karuppagounder SS, Alin L, Chen Y, Brand D, Bourassa MW, Dietrich K, Wilkinson CM, Nadeau CA, Kumar A, Perry S, Pinto JT, Darley-Usmar V, Sanchez S, Milne GL, Pratico D, Holman TR, Carmichael ST, Coppola G, Colbourne F, Ratan RR, N-acetylcysteine targets 5 lipoxygenase-derived, toxic lipids and can synergize with prostaglandin E2 to inhibit ferroptosis and improve outcomes following hemorrhagic stroke in mice, Ann Neurol 84, 854–872 (2018). [PubMed: 30294906]
49. Dave KA, Platel J-C, Huang F, Tian D, Stamboulian-Platel S, Bordey A, Prostaglandin E2 induces glutamate release from subventricular zone astrocytes, Neuron Glia Biol. 6, 201–207 (2010). [PubMed: 21211110]
50. Paniagua-Herranz L, Gil-Redondo JC, Queipo MJ, González-Ramos S, Boscá L, Pérez-Sen R, Miras-Portugal MT, Delicado EG, Prostaglandin E2 Impairs P2Y2/P2Y4 Receptor Signaling in Cerebellar Astrocytes via EP3 Receptors, Front Pharmacol 8, 937 (2017). [PubMed: 29311938]
51. Loynes CA, Lee JA, Robertson AL, Steel MJ, Ellett F, Feng Y, Levy BD, Whyte MKB, Renshaw SA, PGE2 production at sites of tissue injury promotes an anti-inflammatory neutrophil phenotype and determines the outcome of inflammation resolution in vivo, Sci Adv 4, eaar8320 (2018). [PubMed: 30191175]
52. Grainger JR, Wohlfert EA, Fuss IJ, Bouladoux N, Askenase MH, Legrand F, Koo LY, Brenchley JM, Fraser IDC, Belkaid Y, Inflammatory monocytes regulate pathologic responses to commensals during acute gastrointestinal infection, Nat Med 19, 713–721 (2013). [PubMed: 23708291]
53. Tang T, Scambler TE, Smallie T, Cunliffe HE, Ross EA, Rosner DR, O'Neil JD, Clark AR, Macrophage responses to lipopolysaccharide are modulated by a feedback loop involving prostaglandin E2, dual specificity phosphatase 1 and tristetraprolin, Scientific Reports 7, 4350 (2017). [PubMed: 28659609]
54. Buckley CD, Gilroy DW, Serhan CN, Proresolving Lipid Mediators and Mechanisms in the Resolution of Acute Inflammation, Immunity 40, 315–327 (2014). [PubMed: 24656045]
55. Thau-Zuchman O, Shohami E, Alexandrovich AG, Leker RR, Vascular endothelial growth factor increases neurogenesis after traumatic brain injury, J. Cereb. Blood Flow Metab. 30, 1008–1016 (2010). [PubMed: 20068579]
56. Geiseler SJ, Morland C, The Janus Face of VEGF in Stroke, Int J Mol Sci 19 (2018), doi:10.3390/ijms19051362.
57. Gondin J, Théret M, Duhamel G, Pegan K, Mathieu JRR, Peyssonnaux C, Cuvellier S, Latroche C, Chazaud B, Bendahan D, Mounier R, Myeloid HIFs are dispensable for resolution of inflammation during skeletal muscle regeneration, J Immunol 194, 3389–3399 (2015). [PubMed: 25750431]
58. Jung J, Zeng H, Horng T, Metabolism as a guiding force for immunity, Nat. Cell Biol. 21, 85–93 (2019). [PubMed: 30602764]
59. Peruzzotti-Jametti L, Bernstock JD, Vicario N, Costa ASH, Kwok CK, Leonardi T, Booty LM, Bicci I, Balzarotti B, Volpe G, Mallucci G, Manferrari G, Donegà M, Iraci N, Braga A, Hallenbeck JM, Murphy MP, Edenhofer F, Frezza C, Pluchino S, Macrophage-Derived Extracellular Succinate Licenses Neural Stem Cells to Suppress Chronic Neuroinflammation, Cell Stem Cell 22, 355–368.e13 (2018). [PubMed: 29478844]
60. DeMars KM, McCrea AO, Siwarski DM, Sanz BD, Yang C, Candelario-Jalil E, Protective Effects of L-902,688, a Prostanoid EP4 Receptor Agonist, against Acute Blood-Brain Barrier Damage in Experimental Ischemic Stroke, Frontiers in Neuroscience 12, 89 (2018). [PubMed: 29527151]
61. Lobo-Silva D, Carriche GM, Castro AG, Roque S, Saraiva M, Balancing the immune response in the brain: IL-10 and its regulation, Journal of Neuroinflammation 13, 297 (2016). [PubMed: 27881137]
62. Goncalves MB, Williams E-J, Yip P, Yáñez-Muñoz RJ, Williams G, Doherty P, The COX-2 inhibitors, meloxicam and nimesulide, suppress neurogenesis in the adult mouse brain, Br. J. Pharmacol. 159, 1118–1125 (2010). [PubMed: 20136845]
63. Hiruma H, Ichikawa T, Kobayashi H, Hoka S, Takenaka T, Kawakami T, Prostaglandin E(2) enhances axonal transport and neuritogenesis in cultured mouse dorsal root ganglion neurons, Neuroscience 100, 885–891 (2000). [PubMed: 11036222]

64. Nango H, Kosuge Y, Miyagishi H, Sugawa K, Ito Y, Ishige K, Prostaglandin E2 facilitates neurite outgrowth in a motor neuron-like cell line, NSC-34, Journal of Pharmacological Science 135, 64–71 (2017).

65. Goods BA, Askenase MH, Markarian E, Beatty HE, Drake R, Fleming I, DeLong JH, Philip NH, Matouk CC, Awad IA, Zuccarello M, Hanley DF, Love JC, Shalek AK, Sansing LH, Leukocyte dynamics after intracerebral hemorrhage in a living patient reveal rapid adaptations to tissue milieu, bioRxiv, 2020.11.10.375675 (2020).

66. Goods BA, Vahey JM, Steinschneider AF, Askenase MH, Sansing L, Christopher Love J, Blood handling and leukocyte isolation methods impact the global transcriptome of immune cells, BMC Immunol 19, 30 (2018). [PubMed: 30376808]

67. Picelli S, Björklund ÅK, Faridani OR, Sagasser S, Winberg G, Sandberg R, Smart-seq2 for sensitive full-length transcriptome profiling in single cells, Nat. Methods 10, 1096–1098 (2013). [PubMed: 24056875]

68. Robinson MD, Oshlack A, A scaling normalization method for differential expression analysis of RNA-seq data, Genome Biol 11, R25–9 (2010). [PubMed: 20196867]

69. Law CW, Alhamdoosh M, Su S, Smyth GK, Ritchie ME, RNA-seq analysis is easy as 1–2-3 with limma, Glimma and edgeR, F1000Res 5, 1408–29 (2016).

70. Eisenberg E, Levanon EY, Human housekeeping genes, revisited, Trends Genet. 29, 569–574 (2013). [PubMed: 23810203]

71. Reich M, Liefeld T, Gould J, Lerner J, Tamayo P, Mesirov JP, GenePattern 2.0, Nat Genet 38, 500–501 (2006). [PubMed: 16642009]

72. Chen EY, Tan CM, Kou Y, Duan Q, Wang Z, Meirelles GV, Clark NR, Ma'ayan A, Enrichr: interactive and collaborative HTML5 gene list enrichment analysis tool, BMC Bioinformatics 14, 128–14 (2013). [PubMed: 23586463]

73. Kuleshov MV, Jones MR, Rouillard AD, Fernandez NF, Duan Q, Wang Z, Koplev S, Jenkins SL, Jagodnik KM, Lachmann A, McDermott MG, Monteiro CD, Gundersen GW, Ma'ayan A, Enrichr: a comprehensive gene set enrichment analysis web server 2016 update, Nucleic Acids Res. 44, W90–W97 (2016). [PubMed: 27141961]

74. Shannon P, Markiel A, Ozier O, Baliga NS, Wang JT, Ramage D, Amin N, Schwikowski B, Ideker T, Cytoscape: a software environment for integrated models of biomolecular interaction networks, Genome Res. 13, 2498–2504 (2003). [PubMed: 14597658]

75. Gosselin D, Link VM, Romanoski CE, Fonseca GJ, Eichenfield DZ, Spann NJ, Stender JD, Chun HB, Garner H, Geissmann F, Glass CK, Environment drives selection and function of enhancers controlling tissue-specific macrophage identities, Cell 159, 1327–1340 (2014). [PubMed: 25480297]

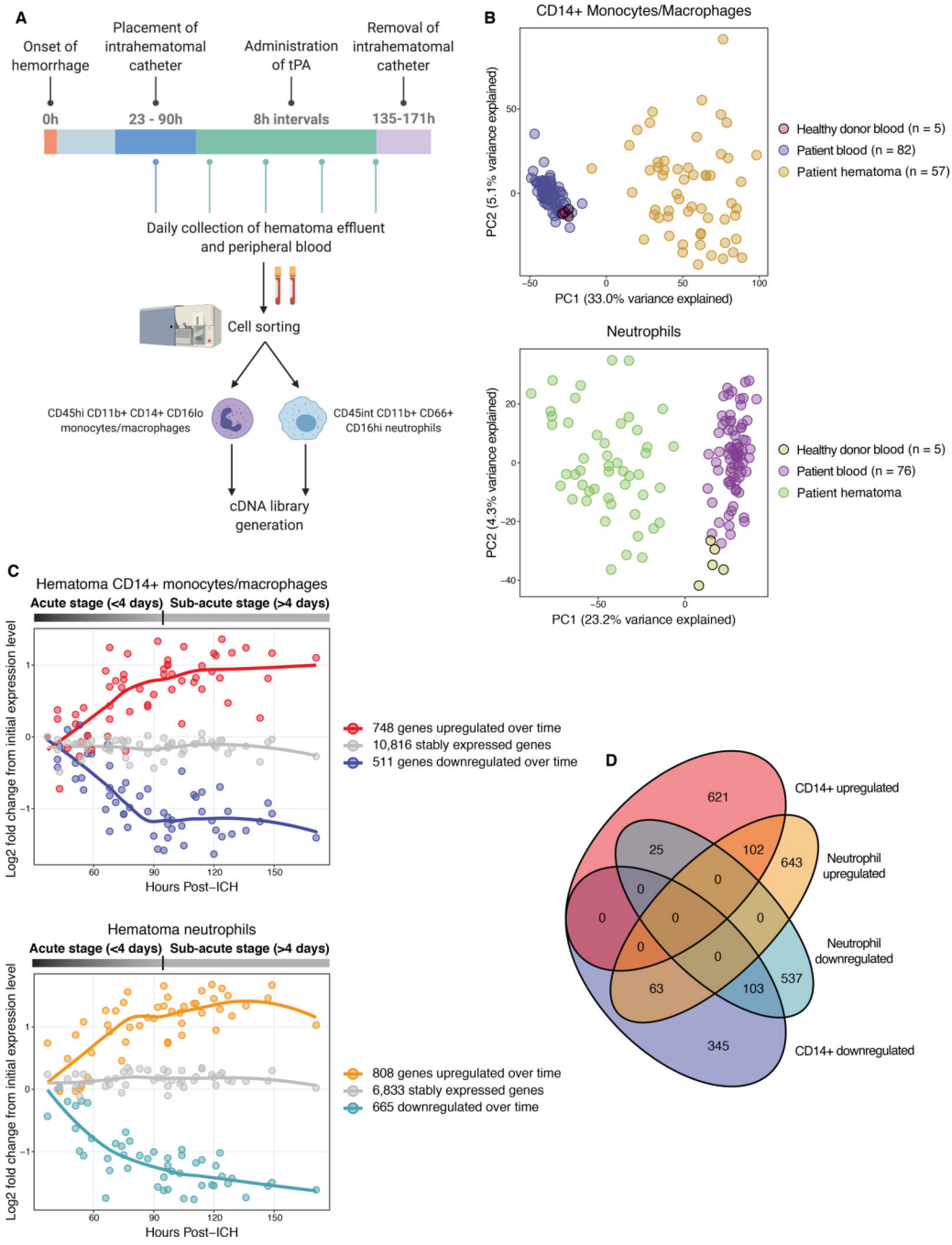

Fig. 1. The myeloid response to ICH is a highly conserved two-stage process.

(**A**) Visual summary of sample collection from ICH patients and cDNA generation for RNA sequencing of myeloid cells from hematoma effluent and peripheral blood. Additional information can be found in Materials and Methods. (**B**) Principal component analysis of transcriptional profiles of CD14+ monocytes/macrophages and neutrophils from ICH patients. Each point represents a single sample; all timepoints from each donor are represented. Projections show the first two principal components, which comprise the largest proportion of the variance in overall gene expression. Additional data are provided in Fig.

S4. (**C**) Mean expression over time of genes in one of two dynamic transcriptional modules identified in hematoma monocytes/macrophages and neutrophils, or in the remaining static genes. Each point represents the mean relative expression level of all genes either upregulated (red/orange), downregulated (blue/teal) or unchanged (gray) over time in a single sample; every monocyte/macrophage or neutrophil sample contributes one point of each color. Colored lines represent loess-smoothed regression of the data. Additional information is provided in Fig. S5. (**D**) Venn diagram depicting overlap in genes between the modules portrayed in (**C**). Gene lists can be found in Table S5.

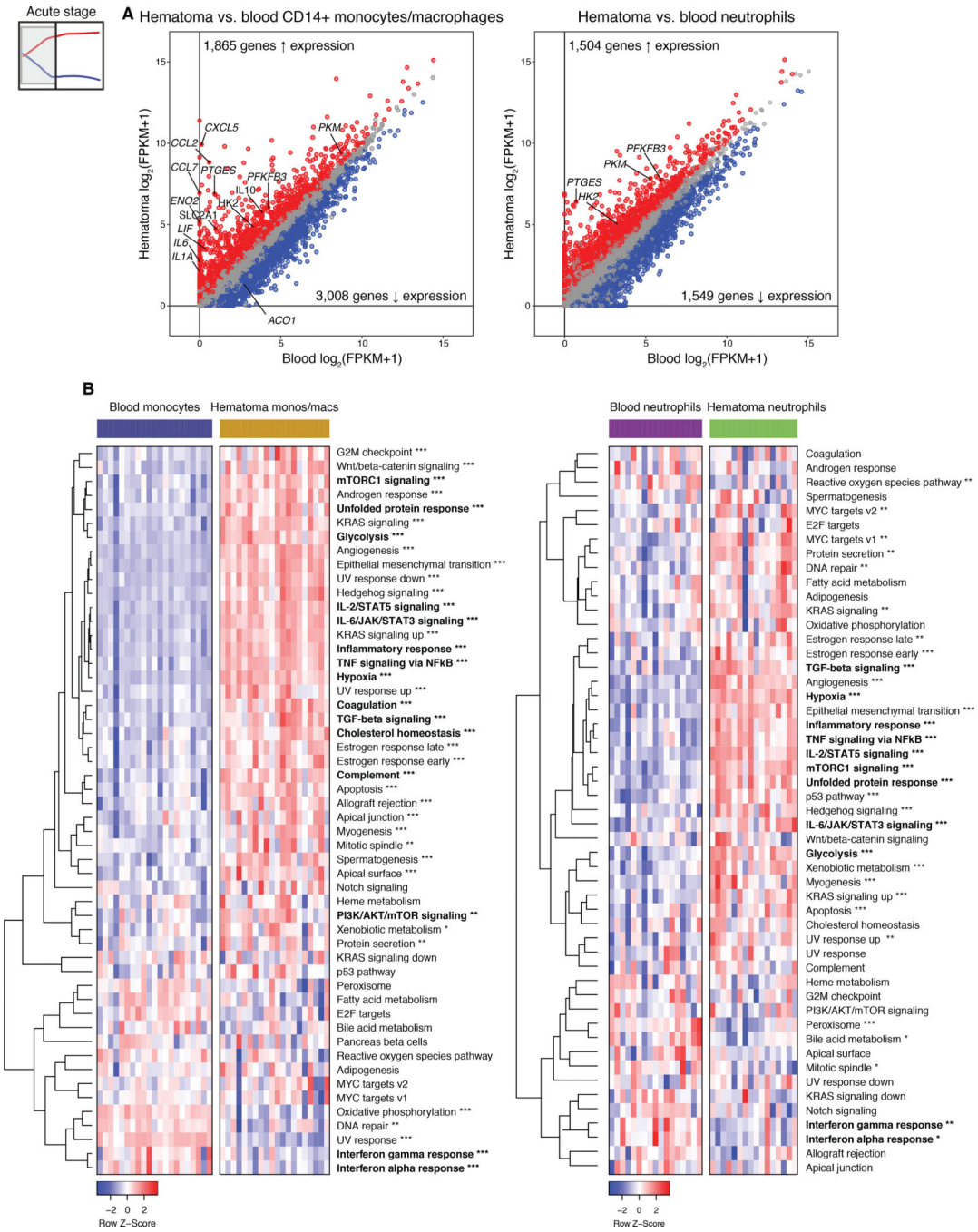

Fig. 2. CD14+ macrophages and neutrophils display broad transcriptional remodeling in the hematoma during the acute stage of ICH.

(**A**) Median level of expression of monocyte/macrophage and neutrophil genes in blood versus hematoma. Only the first (earliest) blood and hematoma samples from each patient in the dataset were included in this analysis, spanning 23 to 99 hours post-ICH; n = 21 patients for monocytes/macrophages, n = 17 patients for neutrophils. Transcriptional profiles that did not meet minimum quality standards were filtered out of the dataset (see Materials and Methods, Initial data processing), which led to fewer neutrophil profiles in the comparison

than monocyte/macrophage profiles. Significantly upregulated or downregulated genes in the hematoma (BH adjusted $p<0.05$) are colored red and blue respectively. (**B**) Single sample gene set enrichment analysis (ssGSEA) of the first blood and hematoma samples from each patient depicting relative enrichment of all 53 hallmark gene sets to provide an overview of transcriptional differences between blood and hematoma cells. Key immune and metabolic pathways are highlighted in bold. Differential enrichment between blood and hematoma populations was assessed by student's t test adjusted for multiple comparisons using the Benjamini-Hochberg (BH) method. ***: $p<0.001$, **: $p<0.01$, *: $p<0.05$.

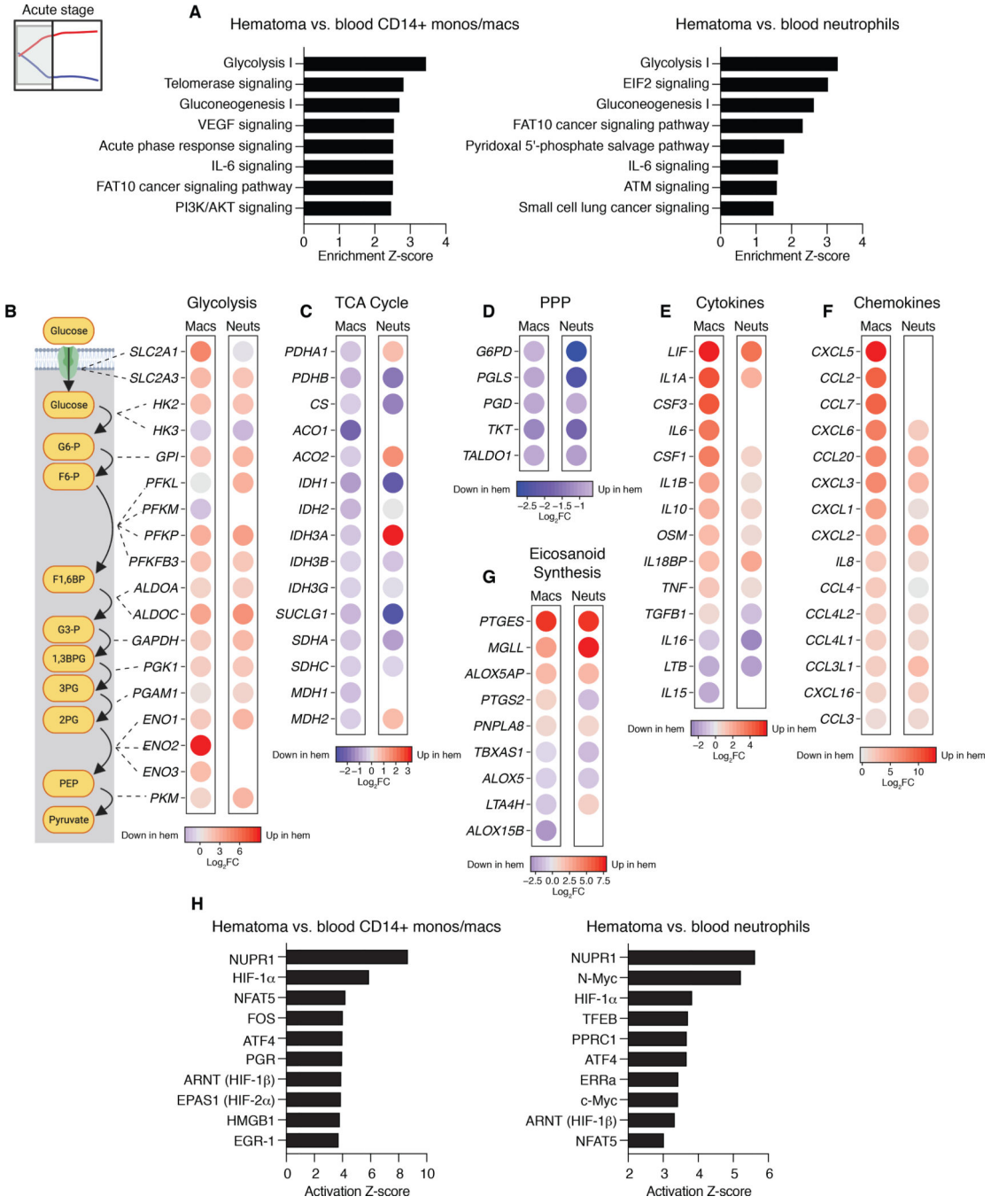

Fig. 3. CD14+ monocytes/macrophages and neutrophils are functionally and metabolically reprogrammed within the hematoma during the acute response to ICH.

(**A**) Canonical pathway analysis of differentially expressed genes in CD14+ monocytes/macrophages and neutrophils during the acute stage. After selecting for pathways with significant enrichment (BH adjusted $p<0.05$), the eight pathways with the highest enrichment Z-scores in each cell type are presented. (**B-G**) Differential expression of genes in glucose utilization pathways and immune factor secretion pathways during the acute stage of ICH. Color scale represents median log2 fold-change in expression in hematoma

compared to blood. Blank spaces represent genes not expressed by neutrophils in either tissue. Only genes with significant differential expression between blood and hematoma in at least one of the two cell types (BH adjusted $p<0.05$) are included. Dashed lines between glycolysis enzymes and schematic denote genes controlling a particular enzymatic step in glycolysis. Heatmaps of expression of these genes by every sample are presented in Fig. S7 and additional differential expression data is presented in Table S6. (**H**) Upstream regulator analysis of predicted transcriptional mediators of the changes to gene expression during the acute stage of the ICH response. After selecting for pathways with significant enrichment (BH adjusted $p<0.05$), the ten pathways with the highest enrichment Z-scores in each cell type are presented. All analyses were performed using the first (earliest) blood and hematoma samples from each patient in the dataset, spanning 23 to 99 hours post-ICH (the acute stage); n = 21 patients for CD14+. monocytes/macrophages, 17 patients for neutrophils.

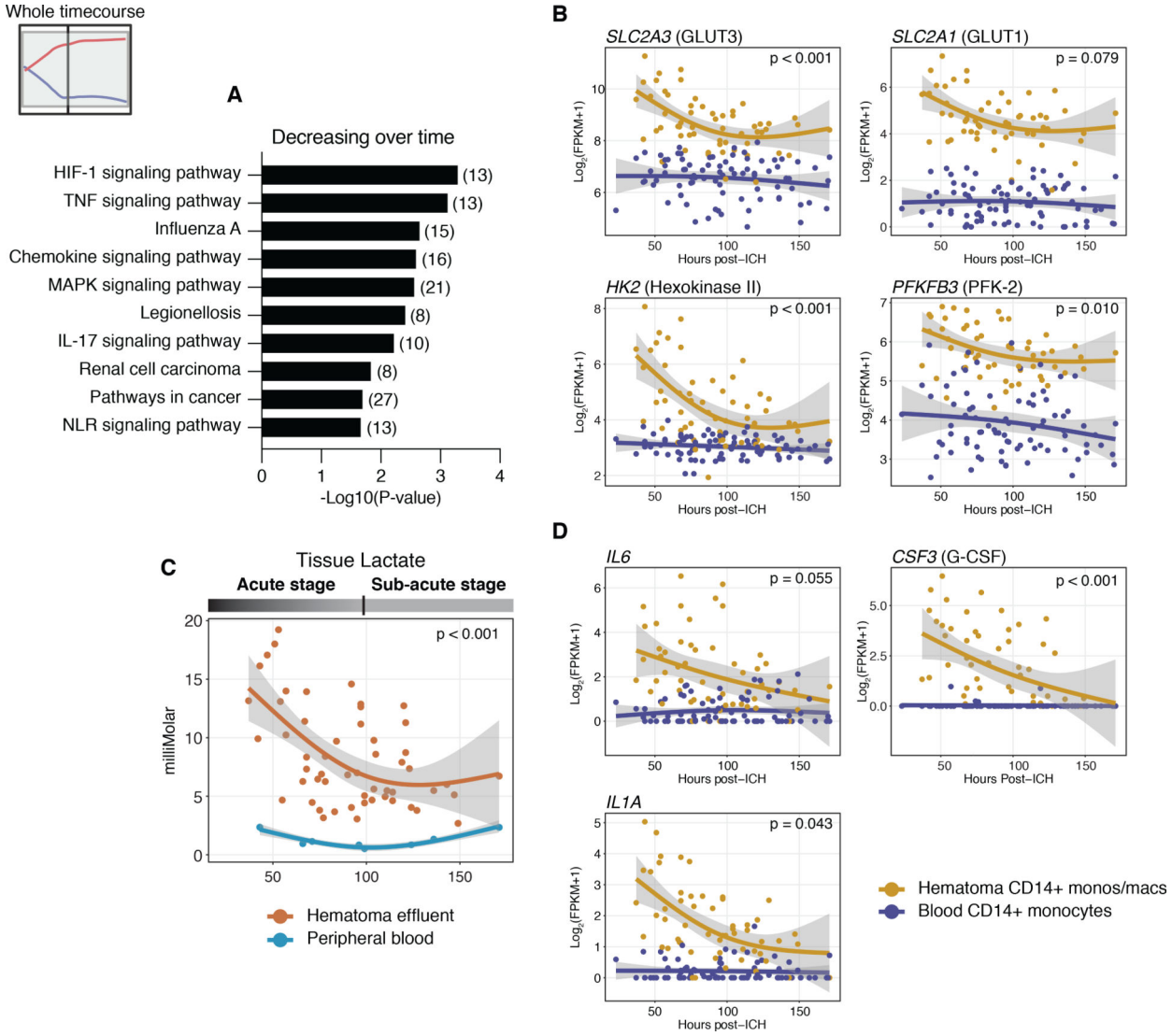

Fig. 4. CD14+ monocytes/macrophages decrease expression of glycolytic and inflammatory genes over time.

(**A**) Gene ontology (GO) analysis of genes decreasing in expression over time in hematoma CD14+ monocytes/macrophages. Number of genes represented in the pathway are presented at the end of each bar. (**B**) Gene expression over time in blood and hematoma CD14+ monocytes/macrophages of enzymes controlling rate limiting steps in glycolysis. Gray shading represents the 95% confidence interval of the regression mean. (**C**) Lactate levels in hematoma effluent and peripheral blood over time after ICH. n = 8 blood samples from 8 patients and 56 hematoma samples from 18 patients. (**D**) Gene expression over time of secreted inflammatory cytokines by blood and hematoma CD14+ monocytes/macrophages. For all gene expression plots, n = 82 (blood) and 57 (hematoma). p values represent significance of changes to gene expression in hematoma cells or lactate levels over time in hematoma as measured by spline regression, adjusted using the BH method. Additional data presented in Table S5 and Fig. S8.

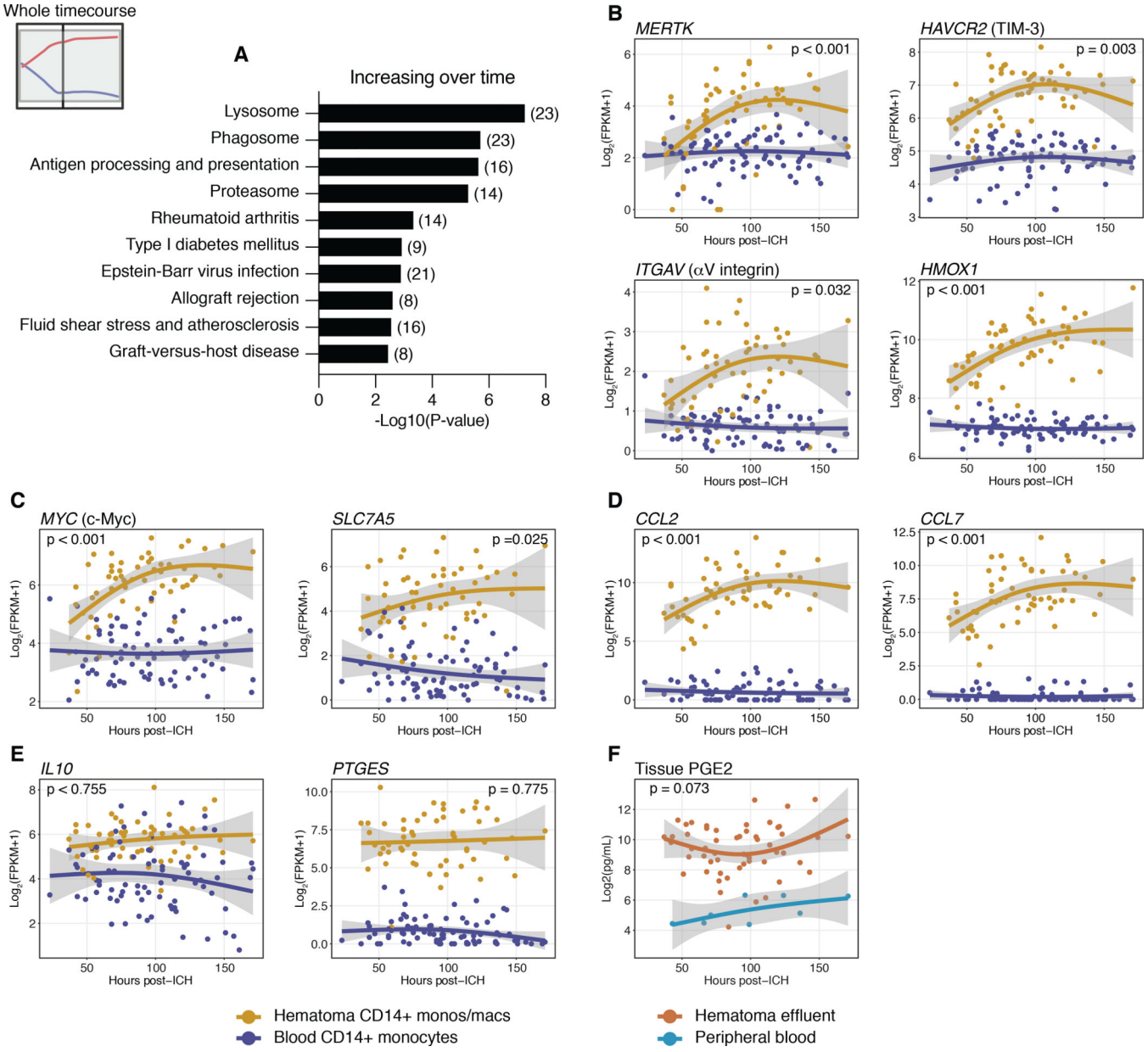

Fig. 5. Hematoma CD14+ monocytes/macrophages acquire a transcriptional profile associated with erythrocyte phagocytosis and repair over time after ICH.

(**A**) Gene ontology (GO) analysis of genes decreasing in expression over time in hematoma CD14+ monocytes/macrophages. Number of genes represented in the pathway are presented at the end of each bar. (**B**) Gene expression over time of genes involved in efferocytosis (*MERTK*, *HAVCR2*, *ITGAV*) and heme degradation (*HMOX1*). (**C-E**) Gene expression over time of genes encoding anabolic metabolism (**C**), monocyte chemoattractants (**D**), the anti-inflammatory cytokine IL-10, and *PTGES* (**E**). Gray shading represents the 95% confidence interval of the regression mean. For all gene expression plots, n = 82 (blood monocytes), 57 (hematoma CD14+ monocytes/macrophages), 76 (blood neutrophils) and 49 (hematoma neutrophils) samples. (**F**) PGE_2 levels in hematoma effluent and peripheral blood over time after ICH. n = 8 blood samples from 8 patients and 57 hematoma samples from 18 patients.

p values represent significance of changes over time as measured by spline regression, adjusted using the BH method. Additional data presented in Table S5 and Fig. S9.

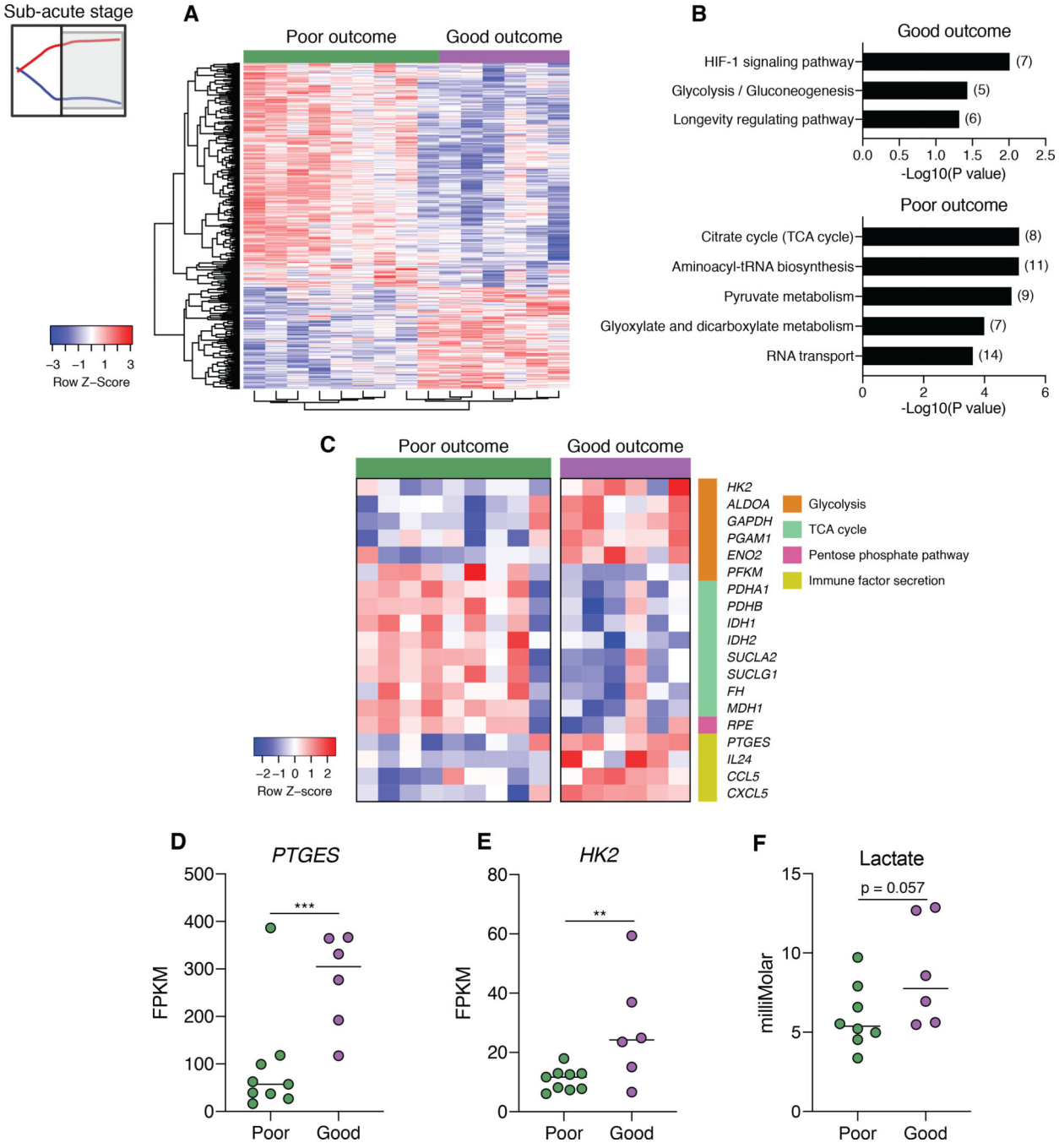

Fig. 6. *PTGES* and glycolytic enzyme genes are more highly expressed by CD14+ monocytes/macrophages in patients with good neurological recovery.

(**A**) Differential gene expression in hematoma CD14+ monocytes/macrophages during the sub-acute stage of ICH (>96 hours post-ICH). Each column represents one patient; each row represents one gene (561 total genes). The dendrogram represents agglomerative hierarchical clustering by unweighted pair group method with arithmetic mean (UPGMA). Additional data presented in Table S9. (**B**) Gene ontology (GO) analysis of differentially expressed genes in hematoma CD14+ monocytes/macrophages during the sub-acute stage of ICH.

Number of genes represented in the pathway are presented at the end of each bar. For enrichment in poor outcome, only the 5 most significantly enriched pathways are shown, additional pathways are presented in Table S10. (**C**) Differentially expressed genes from metabolic and functional pathways in figures 3, 4, and 5 are displayed. (**D**) Expression level of *PTGES* by hematoma CD14+ monocytes/macrophages. (**E**) Expression level of *HK2* by hematoma CD14+ monocytes/macrophages. (**F**) Lactate levels in hematoma during sub-acute stage of ICH; n = 14 total patients, lactate levels for one patient were not recorded. Lactate levels were compared by linear modeling adjusted for initial hemorrhage severity and subsequent F test for statistical significance. For all gene expression data, statistically significant differential expression was determined by linear modeling adjusted for initial hemorrhage severity (n =15 total patients); BH adjusted $p<0.05$ significance threshold. **: $p<0.01$; ***: $p<0.001$,

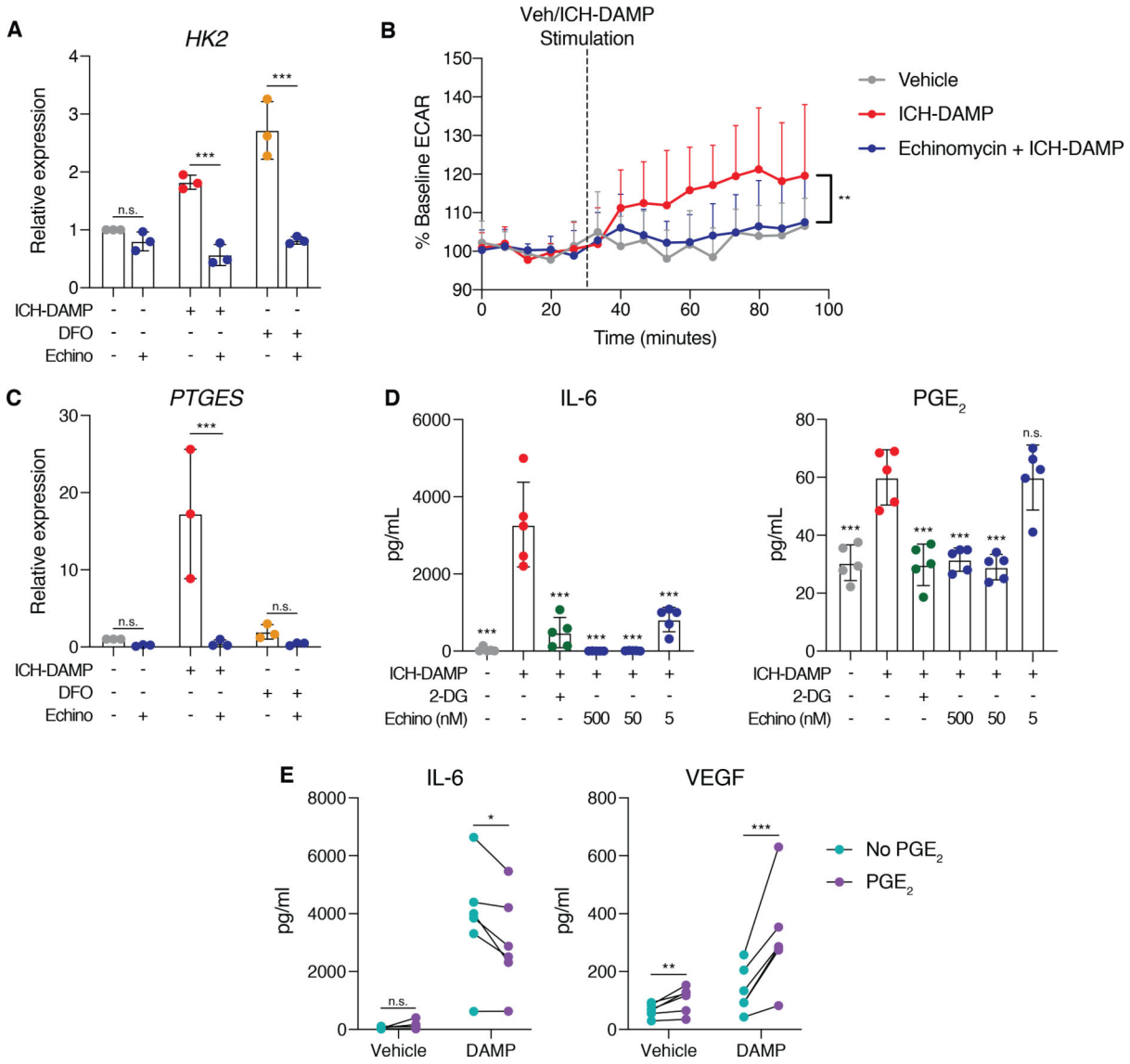

Fig. 7. HIF-mediated glycolysis by macrophages promotes reparative functions.

(**A**) Expression of *HK2* by macrophages treated for 8 hours with ICH-associated danger molecules (ICH-DAMP: S100A8 [1 μg/mL], Thrombin [10 U/mL], and IL-1β [10 ng/mL]), HIF activator DFO (100 μg/mL), or vehicle control +/− HIF signaling antagonist echinomycin (50 nM). Points represent mean values from two replicate wells of n = 3 donors. (**B**) Glycolytic flux of healthy donor human macrophages stimulated with ICH-DAMP or vehicle control in+/− echinomycin (50 nM). Points represent mean values from five replicate wells of n = 4 donors. (**C**) *PTGES* expression by healthy donor macrophages under conditions described in (**A**). (**D**) IL-6 and PGE_2 production by healthy donor macrophages treated for 24 hours with ICH-DAMP or vehicle control +/− echinomycin or glycolysis inhibitor 2-DG (1 mM). All comparisons are to vehicle + ICH-DAMP. (**E**) PGE_2 and VEGF production by healthy donor macrophages treated for 48 hours with ICH-DAMP in the presence or absence of 100 nM PGE_2. Points represent mean values from five

replicate wells of n = 6 donors. Additional cytokine data are presented in Fig. S12. All error bars represent standard deviation. ***: $p<0.001$, **: $p<0.01$